

EMC-Optimized Transparency: Reducing Electromagnetic Emissions in Surveillance Camera Domes

Erik Hansson

Fabian Sondh

June 22, 2023

Master's Thesis in Electrical Measurements at Axis Communications

Supervisor

Johan Nilsson

Supervisor

Johan Gran

Supervisor (Axis)

Isak Stjernrup

Examiner

Lars Wallman



LUND
UNIVERSITY

Faculty of Engineering LTH
Department of Biomedical Engineering

Abstract

Electromagnetic compatibility (EMC) is a crucial aspect to product development. Companies need to make sure their products live up to the standards that exists around the world. One way of reducing electromagnetic emissions is to shield the product, using some conducting material, for instance, copper. An issue arises, though, when transparency is needed, like it is for cameras. At Axis Communications some cameras require a large aperture in its chassis, which increases emissions. This thesis aims to find solutions for transparent shielding of cameras with a dome-surface. This was done by creating prototype shields of different materials. The materials tested are an indium tin oxide film, a silver film, a galvanized steel wire mesh and an aluminium wire mesh. Shielding using aluminium foil with an aperture around the camera lens was also tested.

These prototypes were then evaluated based on reduction of emissions, while taking image quality and cost into account. The electromagnetic emissions were measured both from a comb generator circuit and an Axis camera. A comb generator is a harmonic signal generator that served as a consistent noise source. The measurements were made with near field probes and in an EMC chamber.

The results show that the prototypes manage to reduce emissions across a spectrum, some better than others, using both the comb generator and camera. The materials had varying transparencies, with some being indistinguishable with a regular camera lens. However, all prototypes, except for the aluminium foil with an aperture, had problems with infrared light. Thus, more research is needed before the materials can be implemented on real products.

Acknowledgements

We would like to thank everyone who helped and guided us through this Master's thesis. First, to Isak Stjernrup, our industrial supervisor, who has been there to answer questions and bounce ideas every day at Axis. Secondly, to our academic supervisors, Johan Gran and Johan Nilsson. We thank them for meaningful discussions as well as helping us move forward with our thesis. We would also like to thank Håkan Vikström for helping us order components and materials needed to complete this project. Another thanks goes to Björn Persson for helping us plan and showing us how to do the image measurements in the lab. Our gratitude also goes to Andreas Ericsson who showed us how to use the EMC chamber and gave us some interesting ideas for the thesis. Finally to our friends and family for all their support.

Finally, we would like to thank all the colleagues that helped us with their knowledge and support. We are also grateful to Axis Communications for giving us this opportunity to challenge ourselves and learn, as well as giving us the resources to do this thesis.

List of Abbreviations

AC Alternating current.

CISPR Comité International Spécial des Perturbations Radioélectriques.

DC Direct current.

EMC Electromagnetic compatibility.

EMI Electromagnetic interference.

EUT Equipment under test.

IEEE Institute of Electrical and Electronics Engineers.

IR Infrared light.

ITO Indium tin oxide.

LED Light emitting diode.

PEDOT:PSS poly(3,4-ethylenedioxythiophene) polystyrene sulfonate.

PoE Power over Ethernet.

PWM Pulse-width modulation.

SE Shielding effectiveness.

TCFs Transparent conductive films.

TCMs Transparent conductive materials.

Preface

This thesis was in electrical measurements and was done at Axis Communications between January and June 2023. The figures included in this thesis are made by us, unless explicitly stated. Almost every part of this thesis was done by both authors together. This is because it was done in office at Axis, which made it convenient to do the measurements and writing together. However, there were some different responsibilities. Fabian Sondh was responsible for the prototype building, near field tests and the cost analysis. Erik Hansson had a responsibility for the circuit made in the thesis and its electronics, as well as calculating and drawing the shielding effectiveness graphs. Though, this does not mean that one person did not contribute to the responsibilities of the other.

Contents

1	Introduction	1
1.1	Background	1
1.1.1	Project Definition	2
1.1.2	Thesis Goals	2
1.2	Limitations	3
1.3	Previous Work	3
2	Literature Study	5
2.1	Electromagnetic Compatibility and Interference	5
2.2	Radiated Electromagnetic Emissions	5
2.2.1	Reactive Near Field	6
2.3	Shielding	7
2.4	Transparent Shielding	8
2.4.1	Transparent Conductive Oxides	9
2.4.2	Transparent Conductive Polymers	9
2.4.3	Transparent Conductive Silver	10
2.4.4	Metal Meshes	10
2.4.5	Transparent Conductive Carbon	11
2.5	Electronics	12
2.5.1	Voltage Regulator	12
2.5.2	The Freewheeling Diode	13
2.5.3	Antenna Theory	13
2.6	Standards	14
3	Methodology	17
3.1	Strategy	17
3.2	Harmonic Comb Generator	18

3.3	Prototypes	21
3.3.1	Transparent Conductive Films	23
3.3.2	Conductive Mesh Structures	24
3.3.3	Conductive Polymer	26
3.3.4	Reworked Prototypes for Better Image Quality	26
3.4	Setup	27
3.4.1	Electromagnetic Emission Measurements	27
3.4.2	Image Quality Measurements	33
3.5	Analysis and Evaluation	35
4	Results	37
4.1	Comb Generator	37
4.2	Emissions From Comb Generator	38
4.2.1	No Shielding	39
4.2.2	ITO Film Prototype	40
4.2.3	Silver Film Prototype	41
4.2.4	Galvanized Steel Wire Mesh Prototype	43
4.2.5	Aluminium Mesh Prototype	45
4.2.6	Failed Prototypes	47
4.3	Emissions From the Camera	47
4.3.1	Camera With No Shielding	48
4.3.2	Camera With ITO Film Prototype	48
4.3.3	Camera With Silver Film Prototype	49
4.3.4	Camera With Galvanized Steel Mesh Prototype	50
4.3.5	Camera With Aluminium Mesh Prototype	50
4.3.6	Camera With an Aperture in the Shield	51
4.3.7	From Cable and Camera	52
4.4	Image Quality Tests	53
4.5	Cost Analysis	58
5	Discussion	59
5.1	Strategy and Prototypes	59
5.2	Comb Generator	60
5.3	Reduction of Electromagnetic Emissions	61
5.3.1	Emission Results From the Comb Generator	62

5.3.2	Emission Results From the Camera	63
5.4	Image Quality	65
5.4.1	Visible Light Images	65
5.4.2	Infrared Light Images	65
5.5	Cost Analysis	66
5.6	Future Development	66
6	Conclusions	69
	References	71
7	Appendices	77
A	Comb Generator Emission Graphs	77
A.1	Without a Shield	77
A.2	With an ITO Film Shield	79
A.3	With a Silver Film Shield	80
A.4	With a Galvanized Steel Mesh Shield	81
A.5	With an Aluminium Mesh Shield	82
B	Image Quality Photos	83
B.1	Visual Light Image With No Shield	83
B.2	Visual Light Image With ITO	84
B.3	Visual Light Image With Silver Film	84
B.4	Visual Light Image With Galvanized Steel Mesh	85
B.5	Visual Light Image With Aluminium Mesh	85
B.6	Infrared Light Image With No Shield	86
B.7	Infrared Light Image With ITO	86
B.8	Infrared Light Image With Silver Film	87
B.9	Infrared Light Image With Galvanized Steel Mesh	87
B.10	Infrared Light Image With Aluminium Mesh	88
C	Camera Emission Graphs	89
C.1	Without a Shield	89
C.2	With an ITO Film Shield	90
C.3	With a Silver Film Shield	91
C.4	With a Galvanized Steel Mesh Shield	92
C.5	With an Aluminium Mesh Shield	93

1

Introduction

1.1 Background

As technology advances in both complexity and volume, it becomes more and more crucial to make sure that devices do not interfere electromagnetically with each other. Therefore, a major portion of product development is devoted to making sure that the devices satisfy the directives of the relevant markets. One aspect of these requirements is focused on electromagnetic compatibility, EMC for short, and electromagnetic interference, EMI. On the European Commission's website, it says "The electromagnetic compatibility (EMC) Directive 2014/30/EU ensures that electrical and electronic equipment does not generate, or is not affected by, electromagnetic disturbance" (European Commission 2014). Thus, in order to be able to sell products in the EU market, companies must ensure sufficient immunity and low generation of electromagnetic emissions according to European standard. Similar directives, possibly with different standards, can be found all over the world.

A perfect solution to suppress EMI would be a Faraday's cage, where the device would be shielded from outside noise and result in a reduction of emitted electromagnetic radiation from the device. In a lot of cases, however, this is not a practical way of limiting disturbances. One example of this is surveillance cameras. It is necessary for the optics to be able to see out of the metal chassis which the cameras are mounted on, which increases the difficulty of proper shielding. This difficulty can then lead to sacrifices in, for instance, performance or cost in order to be able to meet the standards. There is, therefore, a widespread interest within the industry in effective and cheap transparent shielding of products.

1.1.1 Project Definition

With this master's thesis, Axis Communications wants to reduce the amount of EMI from its fixed dome cameras, an example of which can be seen in figure 1.1. Specifically, the plastic dome, since that is where the camera needs to have vision. Thus, shielding in this area is difficult and, therefore, an area of interest when it comes to minimizations of electromagnetic interference. Different alternatives were explored for this transparent EMI shielding. Measurements were made on the different options and the results were evaluated from three different perspectives: of cost, of image quality and of attenuation of electromagnetic emissions.



Figure 1.1: An example of a fixed dome camera, P3245-LVE, from Axis and its dome cover.

1.1.2 Thesis Goals

The goals of this thesis can be summarized as the list below.

1. Solutions for transparent shielding will be explored.
2. Prototypes of some solutions will be created and measurements will be made on said prototypes.
3. Clear improvements should be found and evaluated.
4. If number 3 has not been achieved, then clear motivations as to what failed and what can be done to improve the results is necessary.

1.2 Limitations

Since the subject of this thesis work is electrical measurements, and not chemistry nor nanotechnology, the focus will be on solutions and materials that are readily available to buy and test. Some examples are transparent conducting films and easily applied coatings directly on the inside of the dome. So, the process of how to create the materials, implement them and other unrelated material properties might only be described briefly, or not at all. Furthermore, the electromagnetic, EM, emissions will come from a comb generator for a better demonstration of the shielding properties across a large frequency range. Then, similar evaluations are done on one type of camera as well.

1.3 Previous Work

There has been a lot of previous work relating to transparent shielding. Some examples of use cases of such shields are touch screens, windows and OLED screens. One of the dominating transparent materials for these applications is indium tin oxides (Zheng and Kim 2015:1). There has also been a large amount of research in other materials such as graphene (Zheng and Kim 2015; Maurya et al. 2022), silver nano wires (Zhang et al. 2017) and metal meshes (Liang et al. 2022). As such, this topic has been well explored with many existing sources. This thesis aims to fill the gap of applying the different methods to fixed dome security cameras, on or within the dome.

2

Literature Study

This chapter will lay the foundations and provide the background information needed for this thesis. At first, it will go through the basic concepts of EMC and EMI, as well as some methods of how to reduce the emissions. Afterwards, a deep dive into transparent shielding is done in order to give the reader enough information to understand the results and reasoning in the report. Then, the different materials used to shield the camera are explained. As previously stated, how to create the materials will only be briefly mentioned as that information is focused on material science, rather than electrical measurements. Then, some concepts of electronics used in the thesis are explained. Finally, some international standards for electromagnetic interference are explained.

2.1 Electromagnetic Compatibility and Interference

Electromagnetic interference is a sort of environmental pollution of electromagnetic waves, that is, how much electrical devices interfere with each other. Since the amount of electronics in society keeps increasing, it is of utmost importance to keep track of a device's generation of, and immunity against, these kinds of interference. The effects of interference from EM waves varies from crackle in speakers to ignition of flammable materials. Electromagnetic compatibility, or EMC, can be seen as the absence of EMI. A product with good compatibility has strong immunity and low generation of interference (Williams 2017:3). The specific directives, that set the standards of how good compatibility a device should have, is explained in section 2.6.

2.2 Radiated Electromagnetic Emissions

For an antenna that is radiating, the emissions can be categorized into two field regions. Closest to the antenna is the near field, which on its own is repre-

sented as two sub-regions. The reactive- and the Fresnel near field. Further away from the antenna, there is the far field. The far field begins when three conditions are met: Firstly, when the distance from the antenna, R , is greater than or equal to the following equation 2.1. Where λ is the wavelength and D is the largest dimension of the antenna. Secondly, when $R \gg D$ and lastly when $R \gg \lambda$ (Bevelacqua 2022).

$$R \geq \frac{2D^2}{\lambda} \quad (2.1)$$

An electromagnetic field is generated by an electric- and a magnetic field. The electric field, or E-field, is created and proportional to the difference in potential between two conductors. While the magnetic, or H-field, is generated around a conductor and proportional to the current going through it. Which field that is the dominant one, depends on which of the two is the significant one. The ratio of E- to H-field is called the wave impedance (Williams 2017:268). In the far field the H- and E-fields are in phase and orthogonal to each other in the direction of propagation. They can be described as a plane wave with a constant wave impedance of $120\pi \Omega$.

2.2.1 Reactive Near Field

The near field is a complex combination of magnetic- and electric fields (H- and E-fields). As previously mentioned, one of the fields are usually strong when compared to the other in the near field. A high wave impedance signifies that the E-field is dominant, and a low wave impedance signifies that the H-field is dominant. The reactive field is the region closest to the radiation source and is commonly confined by equation 2.2 (Paez B. et al. 2012:110).

$$R < 0.62\sqrt{\frac{D^3}{\lambda}} \quad (2.2)$$

Where D is the largest dimension of the antenna and λ is the wavelength. The H- and E-fields are 90° out of phase from each other in this region, (Bevelacqua 2022), which means that energy is stored instead of dissipated. This can be useful in some applications like RFID or inductive heating but can cause some problems in other scenarios. If, for example in this thesis, the conducting shield is placed close enough to the antenna to be inside the reactive region; then the shield might affect the circuit and cause a change of impedance of the

antenna. This, in turn, might bias the results. Because a change in attenuation with a shield present might be due to this relationship between conductors in the reactive near field, instead of what will be described in section 2.3. This interaction could be different for each material, and shape. Ultimately, this is not a cause of high concern since all attenuation is a positive result for the purpose of this thesis. However, it is an important factor to consider when constructing and evaluating the shields.

2.3 Shielding

Shielding is a rudimentary method, along with filtering, of ensuring EMC. A shield entails a conducting material that is placed around the crucial parts of an electrical device or installation. When an electric field couples to the shield, it will be attenuated before it manages to reach the other side of the conductor. At first, the electric field will induce a current flow on the surface of the shield, which in turn will generate a reflection to the incoming wave. The difference in amplitude of the incoming and reflected wave is called the *reflection loss* (R_{dB}). The current then moves through the shield towards the other edge and as this happens, it is attenuated by the material. This attenuation of current is referred as the *absorption loss* (A_{dB}). Finally, as the current reaches the opposite boundary a second reflection happens. This is usually small in comparison to the other losses and is called the *re-reflection loss* (B_{dB}) (Williams 2017:435-438). Figure 2.1 shows an illustration of this.

To get a notion of how effective a shield is, the shielding effectiveness can be calculated. Shielding effectiveness is a ratio between the field strength with and without the shield. This ratio is highly dependent on the reflections and absorption of the shielding material, and can be defined as follows:

$$SE_{dB} = R_{dB} + A_{dB} + B_{dB} \quad (2.3)$$

Where SE is the shielding effectiveness, R_{dB} is the reflection loss, A_{dB} is the absorption loss and B_{dB} is the re-reflection loss, all of which were described above (Williams 2017:437). It shows how much the signals are attenuated, in dB, by the shield. The reflection loss depends on the wave impedance and the barrier impedance. This means that the shielding effectiveness will differ depending

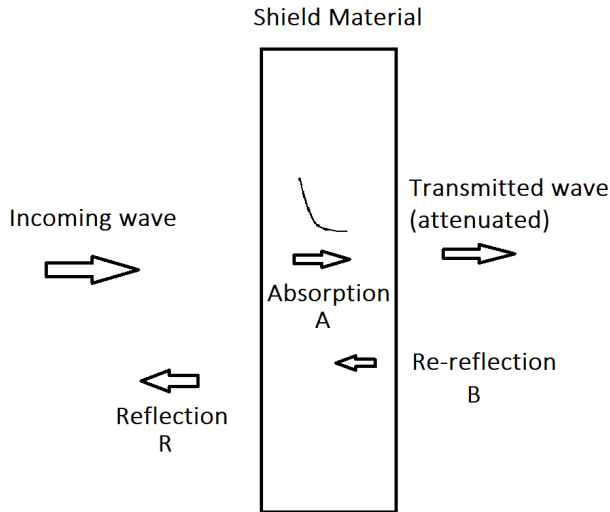


Figure 2.1: Figure illustrating electric shielding. The wave comes towards the shield, one part is reflected, another part is absorbed roughly according to the curve above A. Finally, as the wave changes medium again, a smaller re-reflection dampens some energy from the wave.

on if the electromagnetic wave has a high or low wave impedance. Thus, it depends on whether it is in the far field, or whether the electrical or magnetic field is dominant in the near field. The absorption loss depends on the barrier thickness and its skin depth. The skin depth is an electromagnetic property which confines alternating current flow to the edges of a conductor and, more relevant to this thesis, indicates how deep a field can penetrate a material. This property depends on material properties such as permeability and conductivity, as well as the frequency of the current.

2.4 Transparent Shielding

When it comes to transparent conductive materials, there are many to choose from. Which material one should choose depends on, among other factors, its conductivity, cost, availability of materials, application on substrate and environmental effects. A few keywords that are recurring in articles about transparent conductive materials are: transparent conductive oxide, transparent conductive film, transparent conductive polymers, carbon nanotubes, graphene and

nanowire meshes, all of which are explained in this section. The films are usually specified with a certain transparency and sheet resistance. The sheet resistance has the unit Ohms per square unit area (Ω/sq), which is a constant for each material. The unit does not depend on the size of the sheet, but rather the dimensions of it (Taherian and Kausar 2019:371).

2.4.1 Transparent Conductive Oxides

One option when choosing materials for transparent shielding is indium tin oxide, or ITO. This is one of the most used materials for creating transparent shields. There are a few reasons as to why it is so popular; firstly, the material has great etchability and has a low temperature requirement for this. It also has great transparency and conductivity, which makes it a good candidate for transparent applications. However, there has been a push in finding substitutes to ITO. This is due to indium being considered a critical raw material, even though it is not in short supply on the planet (European Commission 2020; Sveriges Geologiska Undersökning 2020). This, combined with ever increasing use, has driven up the costs of indium by 1000% between 2002 and 2012 (Zheng and Kim 2015:5). It can also be hard to apply the material on flexible surfaces, compared to other alternatives.

2.4.2 Transparent Conductive Polymers

Conductive polymers have some electrical properties that makes them a promising alternative to ITO films. Conductive polymers are organic materials and exists as several different variants. Some of which are: Polythiophene, Polypyrrole and Poly(3,4-ethylenedioxythiophene), or PEDOT. The organic nature of the materials makes them have a less impact on the environment, and less expensive, compared to the ITO alternative. They are also mechanically flexible and light weight, which makes them more suitable for some applications like flexible screens. PEDOT has shown to have an electrical conductivity between 0.5 to 100 S/m , but this can be improved by mixing with some additives like methanol (Zheng and Kim 2015:9-15). The conductivity can be compared to, for instance, copper that has an electrical conductivity of $\sigma = 59.6MS/m$. From reading section 2.3 above, it is known that conductivity is an important element

in the shielding effectiveness. Where a larger conductivity represents a larger attenuation.

PEDOT is a hydrophobic polymer, which means it does not disperse in water solutions. By adding a poly(styrenesulfonate) to PEDOT you get a hydrophilic solution (PEDOT:PSS), which can be dispersed in water. By making it hydrophilic, it becomes possible to disperse the material by using conventional methods like spray deposition. Furthermore, it has a high thermal stability and mechanical flexibility (Xia and Dai 2021:12746), which would work well for the high impact tolerance of the dome.

2.4.3 Transparent Conductive Silver

Another option for transparent shielding is a silver film. Silver is a metal of interest for shielding due to its high conductivity. Silver nanostructures are formed from silver nanoparticles, which in turn is derived from thin silver powder. Silver is a metal of interest for its high conductivity, and nanowires for its high aspect ratio. Nanowires are known to have the highest aspect ratio of all nanostructures. The definition of silver nanowires is based on their shape, with a diameter around 10-200 *nm* and length of 5-100 μm . When used in conductive films, it has a high transmittance of electromagnetic radiation in the visible and part of the infrared range, between 400 to 2000 *nm*. The material can be deposited using a broad range of different techniques, such as spray coating, rod coating and drop/dip coating, which then has to be heated to solidify the coating (Zhang et al. 2017:3).

A conductive film can be made as a hybrid of silver nanowires and graphene. The graphene works as a conducting filler or the apertures in the nanowire network. Likewise, the silver wires contribute to defects in the graphene layer, where a boundary have arisen, and its sheet resistance is increased (Zhang et al. 2017:18).

2.4.4 Metal Meshes

In order to make transparent metals for shielding, one can use a grid or mesh of metal. The resulting shielding effectiveness depends on the density of the mesh; where a denser mesh is better as a shield but sacrifices transparency (Mardigu-

ian et al. 2017:242). Since the metal mesh is not a smooth continuous surface, but rather has several apertures, the expression for shielding effectiveness needs to be modified. A simplified model of the shielding effectiveness of a mesh structure, is equation 2.4. The equation will be used as the theoretical shielding effectiveness, which will be compared to the measured results.

$$SE = 20 \cdot \log(\lambda / 2L) - 20 \cdot \log(\sqrt{n}) \quad (2.4)$$

Where SE is the shielding effectiveness, λ is the wavelength, L is the longest dimension of the apertures and n is the number of apertures (Williams 2017:439, 453-454). As the source states, this is only a rough estimate and should be used when evaluating design options. Thus, the absolute numbers could be off compared to the measured ones.

According to a study that measured the shielding effectiveness depending on the amount of lines per wavelength, the optimal number of lines is around 5-7 lines per wavelength (Duffy et al. 2015:1268). With this stated, smaller apertures will be evaluated for comparison. According to a manufacturer, a minimum aperture of 50 times less than the wavelength is the rule of thumb, which would mean an aperture length of, e.g., 6 mm for a wavelength of 30 cm (Fenical n.d.).

2.4.5 Transparent Conductive Carbon

Carbon Nanotubes

When it comes to transparent conductive carbon, one of the prominent materials is carbon nanotubes, or CNT. An important characteristic of a CNT material is its aspect ratio, which is the ratio between its highest and lowest dimension. Where a higher aspect ratio improves its shield effectiveness. Carbon nanotubes has been regarded as one of the most promising candidates for transparent conductive films for a long time (Urper et al. 2017:213-214). Research has showed sheet resistances of 100 – 300Ω/sq and transparencies of 70 – 90% (Zheng and Kim 2015:18; Park et al. 2020:2). Research has also found that covering multi-walled carbon nanotubes with PEDOT increases its electrical conductivity in polymers (Zhou and Lubineau 2013:6199).

Graphene

More recently, graphene has been researched as a candidate for replacing ITOs, which was described in section 2.4.1, as the dominating transparent conductive film. The unique atomic structure gives the material some interesting properties while keeping a high transparency, as high as 97% (Zheng and Kim 2015:19). Sheet resistance can be quite high but can be reduced by chemical doping.

The unique property of graphene comes from the fact that it is made up by a two-dimensional, one atom thick, honeycomb lattices. The properties include high-charge carrier mobility, quantum Hall effect in room temperature, etc. Graphene stays transparent over a wider bandwidth compared to ITO, silver wire nanotubes and thin metallic films.

2.5 Electronics

2.5.1 Voltage Regulator

A voltage regulator is a device which purpose is to maintain a constant voltage on its output. This can be done in a variety of techniques; feed-forward or negative feedback and electro-mechanical mechanisms or electronic components. A switching feedback regulator with electronic components was used in this project. These regulators work by using the output voltage as feedback and comparing it to some reference value, 5 V in this thesis. The difference of these voltages is then used by the controller to adjust the output voltage towards the reference voltage. It accomplishes this by taking the amplified error and comparing it with a suitable oscillator in a comparator. Then it uses this signal as a driver for the switch, in this case a transistor, so the switching will change slightly, resulting in a correction of the output voltage. Figure 2.2 shows a block diagram of the voltage regulator used in this thesis.

When looking at this kind of voltage regulators from an EMC standpoint, they are quite noisy (Williams 2017:263). The noise comes from the rapidly switching on and off inside the regulator. This switching controls the output voltage based on pulse-width modulation, or PWM, that modulates the signal to the wanted shape (Barr 2001; Erickson and Maksimović 2007:253-256). This noise can cause the circuit to become unstable, and some measures should,

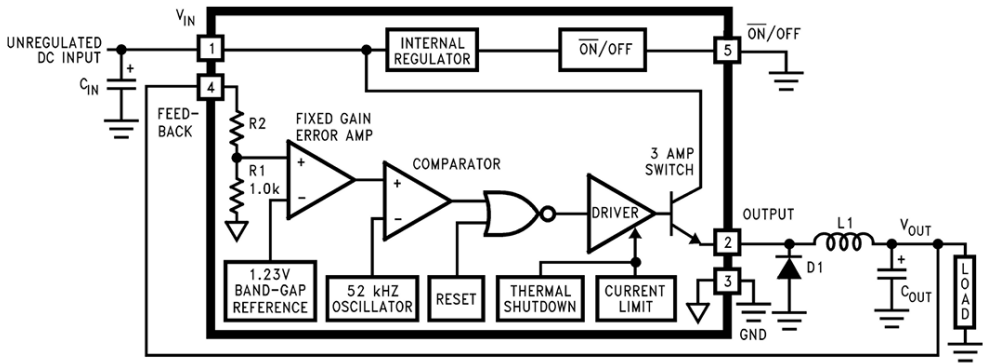


Figure 2.2: A block diagram of the voltage regulator LM2576 (Texas Instruments 1999).

therefore, be taken to reduce these disturbances. The measures taken in this thesis are explained in section 3.2.

2.5.2 The Freewheeling Diode

In applications where switching occurs together with a DC load on a inductance, a freewheeling diode could be useful. The voltage across an inductor can be described as the following:

$$v(t) = L \frac{di}{dt} \quad (2.5)$$

Where $v(t)$ is the voltage, L is the inductance and $\frac{di}{dt}$ is the derivative of the current with respect to time (Hambley 2014:159). Thus, if the flow of current is rapidly cut, the derivative will have a large negative value and a large negative voltage will occur over the inductor. In order to keep the current flowing, and in turn avoiding damage to the components, a freewheeling diode can be connected from ground to the inductor (Erickson and Maksimović 2007:65-67). This is sometimes also called flyback- or catch diodes.

2.5.3 Antenna Theory

When performing tests on radiating EMI, antennas become relevant. An antenna is a transducer that receives or transmits electromagnetic waves. When receiving, the antenna intercepts the waves and converts the power into electricity. There are several different types of antennas, e.g., monopole-, dipole-

and array antennas. There are some important characteristics that one needs to consider when using an antenna. One of which is the bandwidth. The bandwidth describes the frequency range which the antenna can efficiently operate at. This can be wide or narrow (Visser 2012:5, 81-96).

There are also some other important aspects when using an antenna as a transducer. The electric field strength, (E), that is measured has the unit $dB\mu V/m$, while in the spectrum analyzer, (V), is in $dB\mu V$. Additionally, there is an attenuation, (A), in dB in the cable between the antenna and spectrum analyzer. There is also an antenna factor, (AF) in dB/m ; an antenna has an attenuation depending on the frequency. Equation 2.6 shows the relationship between these factors (Williams 2017:151).

$$E [dB\mu V/m] = V [dB\mu V] + AF [dB/m] + A [dB] \quad (2.6)$$

The measurement setup needs to take this into account in order to get reliable results.

2.6 Standards

There are some international standards for what level of EMI a device may emit and should have immunity to. One of these international standardization organizations is the International Special Committee on Radio Interference (CISPR). Some relevant standards in Sweden that are based on CISPR standards are the Electromagnetic compatibility of multimedia equipment - Emission requirements SS-EN 55032 (Swedish Standards Institute 2015). Also, the Electromagnetic compatibility (EMC) - Part 6-3: Generic standards - Emission standard for residential, commercial and light-industrial environments SS-EN 61000-6-3 (Swedish Standards Institute 2007). Radiated electromagnetic emissions have two different classes, class A and class B (Williams 2017:41-42). These have different limits as to how high the emissions are allowed to be. Class A is relevant when the device is marketed for commercial, industrial or business use, while class B is relevant for domestic use. Since the market of the cameras from Axis is mostly for businesses, class A is used as reference in this thesis, and by Axis in their tests.

The standards of interest are for radiated emissions; there also exists standards for conducted emissions but they are not relevant for this thesis. In the

figures 2.3 and 2.4, the radiated limits can be seen. In the EMC chamber at Axis, the distance between the EUT and antenna is 3 m. When measuring the full frequency spectrum with a spectrum analyzer, there exists a few parameters that are used to ensure accurate readings. The parameters can be seen in figure 2.5.

Quasi-peak

These measurements require a detector function to register the emissions. Quasi-peak is one of these detector functions. In contrast to a peak detector, that follows the envelope of the signal, a quasi-peak detector detects peaks using weighted charge and discharge times. This will result in slightly lower peaks for modulated and pulsed signals. The detector was originally used because it seemed to be a better indicator for subjective annoyances, experienced when listening to radio broadcasts (Williams 2017:145-146).

Table clause	Frequency range MHz	Measurement			Class A limits dB(μ V/m)
		Facility (see Table A.1)	Distance m	Detector type / bandwidth	
A2.1	30 to 230	OATS/SAC	10	Quasi Peak / 120 kHz	40
	230 to 1 000				47
A2.2	30 to 230	OATS/SAC	3		50
	230 to 1 000				57
A2.3	30 to 230	FAR	10	42 to 35	
	230 to 1 000			42	
A2.4	30 to 230	FAR	3	52 to 45	
	230 to 1 000			52	

Figure 2.3: Radiated emission limits below 1 GHz (Swedish Standards Institute 2015).

Table clause	Frequency range MHz	Measurement			Class A limits dB(μV/m)
		Facility (see Table A.1)	Distance m	Detector type / bandwidth	
A3.1	1 000 to 3 000	FSOATS	3	Average / 1 MHz	56
	3 000 to 6 000				60
A3.2	1 000 to 3 000			Peak / 1 MHz	76
	3 000 to 6 000				80

Figure 2.4: Radiated emission limits above 1 GHz (Swedish Standards Institute 2015).

CISPR band				A	B	C, D	E
Band edge (CISPR)				9–150kHz	0.15–30MHz	30MHz–1GHz	1–18GHz
Band edge (Military)							
	20Hz–1kHz		1–10kHz				
Bandwidth at -6dB points							
CISPR	N/A		N/A	200Hz	9kHz	120kHz	1MHz
Military	10Hz		100Hz	1kHz	10kHz	100kHz	
Quasi-peak detector							
Charge time constant, ms				45	1	1	N/A
Discharge time constant, ms				500	160	550	
Overload factor, dB				24	30	43.5	

Figure 2.5: Bandwidths (Williams 2017:144).

3

Methodology

This section will describe the process that the project followed. At first, the general strategy of this thesis is explained. Then, the process of creating the harmonic comb generator is explored. Afterwards, a walk-through of how the measurements were setup is done, so that they can be followed, and the results reproduced. Finally, some words on how the analysis is done, to give the reader some context of the results in the next chapter.

3.1 Strategy

Using transparent conductive materials for EMC purposes is not a new concept. It exists in many applications where optics are important. Materials used or developed for this use case was explored in the previous chapter. It became apparent that the materials in question would not only need to have a low sheet resistance for the shielding effectiveness. But moreover, be able to form a layer across the inside, or outside, of the dome and stick to polycarbonate, which was the material of the original dome. Because of the lack of knowledge in material science of coatings, no dome was coated with these materials. Instead, sheets with these materials coated on top of them were bought and retrofitted on top of the dome; or the material was used as the dome itself. With this said it is still important to note that there are methods in the scientific literature of application methods on polycarbonate. Some of which are, Chemical Vapor Deposition (Chandler 2015), spin coating (Fakirov 2016) and drop casting (Kaliyaraj Selva Kumar et al. 2020). After the emissions were measured, the image obstruction by the shields was evaluated. A camera was also evaluated with the different prototypes, in order to see the shielding effects in a more realistic scenario.

3.2 Harmonic Comb Generator

Since the cameras are well made and thoroughly tested, they only let out a small amount of radiation. This meant that it can be difficult to see a substantial difference before and after shielding on the device. Therefore, a harmonic comb generator was created as a source of noise. Near field test on a camera and on the comb generator were done to ensure that both had the same dominant field. The comb generator is a device that produces a signal with harmonics. In the frequency domain, these harmonics are represented as evenly spaced spikes that can be likened to a comb. Figure 3.1 shows a circuit diagram of the comb generator used in this thesis.

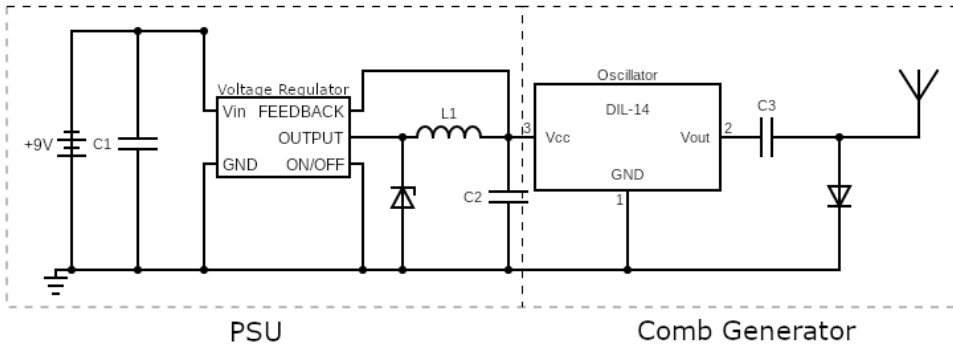


Figure 3.1: A simple comb generator. Divided into two parts: power supply (PSU) and comb generator. Each part is explained below.

The generator was powered by a 9 V battery, which removed the interference coming from cables, so that the focus of the emission attenuation was on the dome. The chosen oscillator was the DIL-14, which oscillates at 10 MHz with a duty cycle of 50% and is driven at 5 V DC. In order to get 5 V DC to the oscillator, a voltage regulator was used. Figure 3.2 shows the power supply of the circuit. A regulator has the advantage that it can keep consistent voltage on the output; while the input has decreasing voltage, which is the case for a battery. The chosen regulator is LM2576 (Texas Instruments 1999). The regulator, which was explained in section 2.5.1, is switched and the output will therefore be noisy. To counteract this, a low pass filter was connected to the output of the regulator, in accordance with the data sheet. The filter consists of an inductance

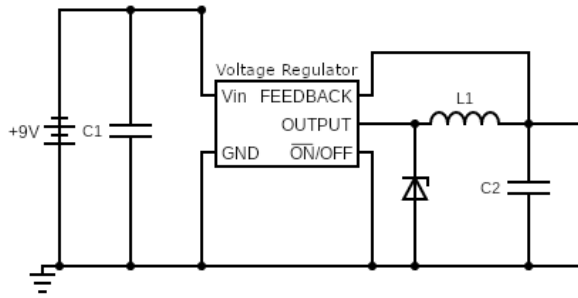


Figure 3.2: Power supply, consisting of a battery, some filter components and a voltage regulator.

in series and a capacitor connected to ground. Since the inductor has a lower impedance for low frequencies (Hambley 2014:156-157) and the capacitor has a high impedance for low frequencies (Hambley 2014:145), and vice versa; the filter will let the DC signal through while the higher frequencies are blocked or connected to ground. This filter will, therefore, reduce the ripple and noise coming from the switching. The component values were chosen based on the data sheet. A Zener diode was also connected as a flyback diode, which was described in section 2.5.2, between ground and the output of the regulator because of the inductance in the output. In figure 3.3, the comb generator part of the circuit can be seen.

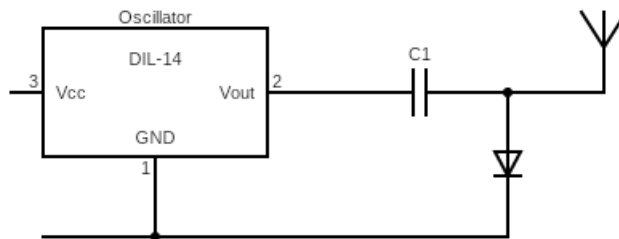


Figure 3.3: The harmonic comb generator.

As previously mentioned, the oscillator generated a signal of 10 MHz , when supplied with 5 V DC . This signal was a square wave that went through a capacitor. The capacitor blocks DC and lets higher frequencies through. This meant that when the square wave was low or high, the capacitor served as an open circuit. While during the slopes, where the frequency is high, it served as a short circuit. Thus, the capacitor can be seen as a differentiator to the oscillation and the resulting signal consisted of spikes, originating from each slope. This differentiation depends on the time constant of the circuit. In the frequency spectrum, a fundamental frequency of 10 MHz and the harmonics could be seen. The purpose of the diode was to decrease the rise- and fall time of the slopes, which increases the amplitude of peaks with higher frequencies (Kenneth 2015:55-56).

Finally, a dipole antenna consisting of two 7.5 cm copper cables was connected, one part after the output-capacitor and another part to ground. The size of the antenna was limited by the dimensions of the dome. A larger antenna would be optimal for better signal emission efficiency, however, testing showed that the smaller antenna was sufficient for the intended task. It is important to note that the components on the output side of the board should be close together, for a lower signal loss. The board and the chassis share a common ground at the negative 9 V node. Figure 3.4 shows the resulting comb generator. The underside of the comb generator was covered by electric tape for electrical isolation from the chassis. The signal coming to the antenna was measured using an oscilloscope with the circuit ground as a reference point. The oscilloscope used was RIGOL MSO5204, with a sampling rate of 8 GSa/s and a bandwidth of 200 MHz .

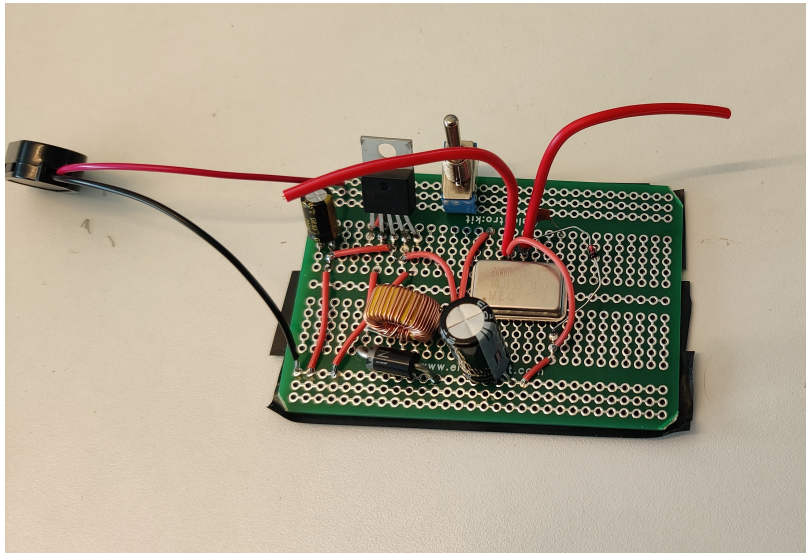
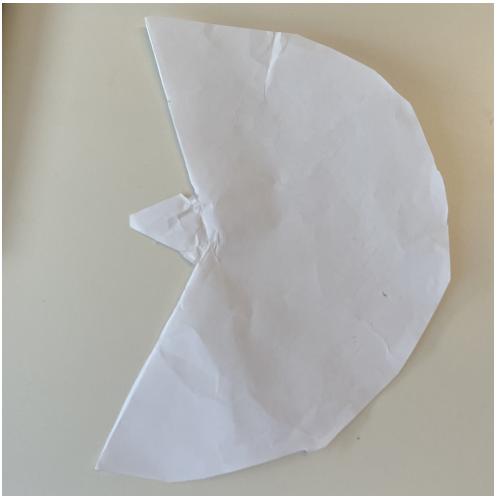


Figure 3.4: The resulting harmonic comb generator. A battery is connected to the connector to the left, with the black cable going to ground and red cable going to +9 V. The antenna consists of a small makeshift dipole antenna (two 7.5 cm cables). The silver rectangle is the oscillator and the black component with five legs is the voltage regulator.

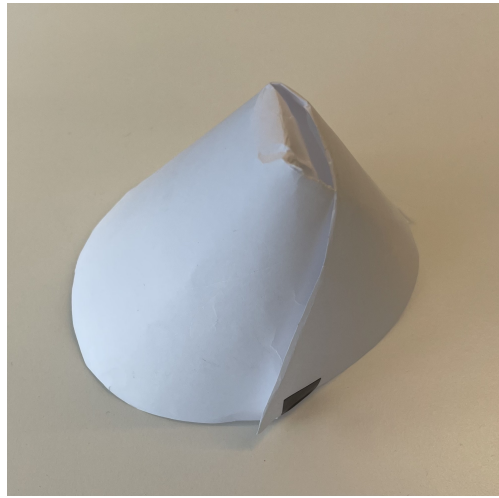
3.3 Prototypes

Here, the process of constructing the different prototypes is explained. The materials are divided into two groups: transparent conductive films, or TCFs, and conductive mesh structures. A template was constructed in paper, which was later used to make the shields. The shields were folded into a cone as seen in figure 3.5a and 3.5b. Then, joined together with copper tape at the seam and bottom for complete conductivity for the shield and chassis. Lastly, electrical tape was also applied at the seam to improve the structural integrity.

Not all the materials that were researched in the literature study could be tested. This was either because there was no supplier for the material or there was no easy way of applying it to either the dome or onto a film.



(a)



(b)

Figure 3.5: The paper template that was used when creating the shields.

3.3.1 Transparent Conductive Films

The TCFs used for shielding were an indium tin oxide film and a silver alloy film. The materials were coated on top of a flexible, but flat material. This meant that they had to be formed into a dome, in order to emulate the real application. The template that was previously described was used for this purpose. This gave the different materials the same shape and, thus, a more reliable result. One side of the prototype dome had to be connected to itself, so that it acted as a solid dome, which gave better results and mirrored a real application better. The ITO film was subcontracted to the company Sigma-Aldrich. The dimension of the film was $348 \times 348 \times 0.152 \text{ mm}$ and its sheet resistance was between 45 and $65 \text{ } \Omega/\text{sq}$. The silver material was made by TDK Corporation, had the dimensions $210 \times 297 \times 0.125 \text{ mm}$ and a surface resistivity of $3.7 \text{ } \Omega/\text{sq}$. The ITO and silver film prototypes are shown in figure 3.6a and 3.6b, respectively.

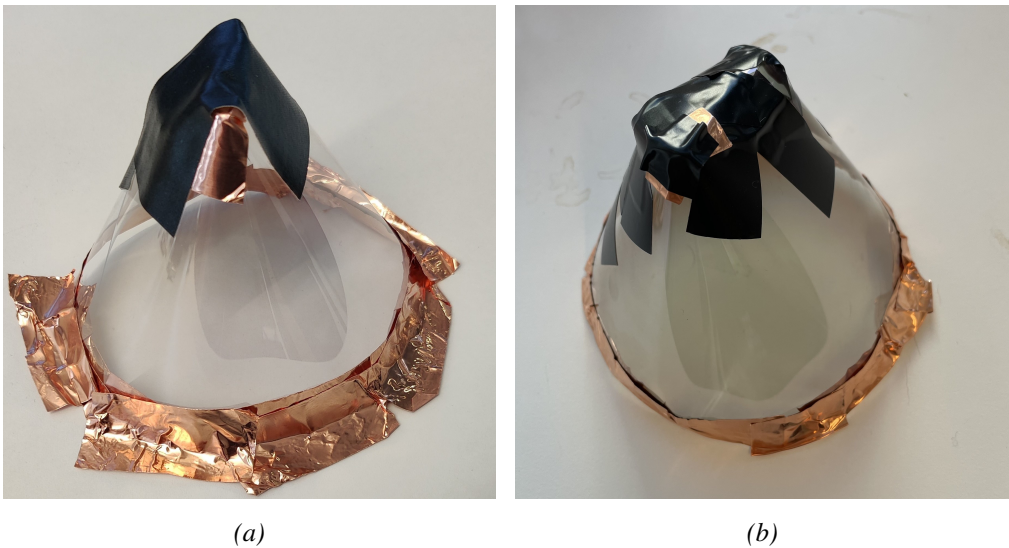


Figure 3.6: ITO (3.6a) and Silver (3.6b) prototype shield. The transparent part is the transparent conductive film, the black tape is regular electric tape used to keep the structure intact and the copper tape is used for connecting the shield to itself and to the chassis.

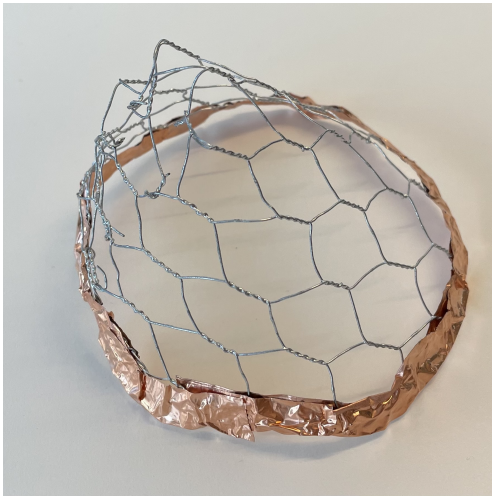
3.3.2 Conductive Mesh Structures

There were three different materials formed as a mesh used in the thesis. The first, was a standard galvanized steel mesh, i.e., steel with a protective coating of zinc. Galvanized steel has a resistivity of roughly $1.7 \cdot 10^{-7} \Omega m$. The wire mesh had an aperture size of 20 mm^2 . Figure 3.7a shows this prototype. The second prototype was a net made of aluminium. It had an aperture size of $2 \times 3 \text{ mm}$ and a wire thickness of 0.4 mm . The resistivity of aluminium is about $2.8 \cdot 10^{-8} \Omega m$ (Williams 2017:522). This prototype is shown in figure 3.7b. Finally, there was the conductive ink. Since the ink was not transparent, it was painted in a mesh like pattern on top of the existing dome. According to the data sheet, the resistance of the paint can be calculated with the following equation:

$$R = 19.77 \left(\frac{l}{w} \right) + 12 \quad (3.1)$$

Where R is the resistance, l is the length and w is the width. The largest aperture size of the pattern was 2.5 by 3 cm and is shown in figure 3.8.

The resistance of the three meshes were measured with a multi-meter. Of the three only the ink mesh was not highly conductive. Which became apparent when looking at the resistivity of the three materials. For the ink, the resistance is given by equation 3.1. The equation says the lowest resistance is with a length to width ratio of 1:1. Which gives a resistance of 32Ω . While the two metal meshes has a factor of ten to the power of 8 or 9 lower resistivity.



(a)



(b)

Figure 3.7: Galvanized steel mesh (3.7a) and aluminium mesh (3.7b) prototype shields. The black tape is regular electric tape used to keep the structure intact and the copper tape is used for connecting the shield to itself at the seams and to the chassis.



Figure 3.8: Ink mesh prototype shield coated on a camera dome, copper tape for galvanic connection.

3.3.3 Conductive Polymer

The dome is made from polycarbonate and was cleaned with 99% isopropyl alcohol. No other treatment was made on the dome. The application method for the polymer liquid on the dome was spin coating, by hand. Then placing it in the oven for 10 minutes at 100° C. As can be observed in figure 3.9, this did not work. The liquid was too thin and did not stick to the dome. As described in the literature study, there are other methods of coating. As an example, spin coating could work with the correct equipment.



Figure 3.9: PEDOT:PSS prototype shield painted on a camera dome.

3.3.4 Reworked Prototypes for Better Image Quality

One way of shielding, while keeping the integrity of the visibility, is covering the camera completely, but with an aperture for the image sensors. The image quality is then preserved and, since the smallest relevant wavelengths are still quite long compared to the dimensions of the camera, the attenuation should still be high. A promising result in these trials could eliminate the need for transparent materials and, thus, increasing the number of material choices. Figure 3.10 shows the prototype for this.



Figure 3.10: Aluminium foil shield without lens obstruction.

3.4 Setup

This section describes the different setups used in the tests. The goal is for the reader to be able to replicate the measurements in order to validate the results and conclusions made in the report.

3.4.1 Electromagnetic Emission Measurements

After the literature study, materials for prototypes were ordered and then measured for their effectiveness. At first, the comb generator was measured without any shield and this data were later used as a reference. Then the different materials were applied to cover the dome and new measurements were made. Then, the same procedure for a camera was done. This gave some perspective of how real products could react to shielding.

Thereafter, measurements using near field probes and a spectrum analyzer were made. This gave some understanding as to how the shield affects the camera emissions, in the reactive near field which was explained in 2.2.1. Figure 3.11 shows the two probes used to determine the dominant near field of the camera and comb generator. The spectrum analyzer which was used for this

was a Keysight N9322C. The sweep time was 1.89 s, the filter bandwidth was 100 kHz, and it was measured using continuous sweeping. The reason 100 kHz was used as the filter bandwidth, and not 120 kHz as the standard suggests, was that it was not possible on the specific spectrum analyzer which was used.



Figure 3.11: Two near field probes constructed by us. The above one is an E-field and the bottom one with the loop is the H-field probe.

EMC Chamber

The tests and measurements were done in a special chamber called an EMC chamber, which can be seen in figure 3.12. The purpose of the chamber is to reduce outside electromagnetic influences on the testing inside the chamber and, thus, imitating a free field measurement. The room accomplished this by shielding the room, which attenuated the outside signals. One potential problem with this, is that a standing wave could occur inside the chamber. To account for this, absorbents are placed on the walls, floor and ceiling. This reduces the wave reflections and standing waves. These absorbents are, therefore, always used in EMC chambers for emission measurements. To eliminate even more influences, a battery was used to power the camera and comb generator. This is because it would remove interference from the power over Ethernet (PoE) cable. Inside the chamber, there were antennas and the equipment under test, EUT, for evaluation. During operation, all emissions were collected by the antenna and analyzed by a spectrum analyzer. Outside the chamber a computer analyzed the measurements with a software named EMC32, which is developed by Rohde & Schwarz. Figure 3.13 shows a flow chart of the setup used in the emission measurements.

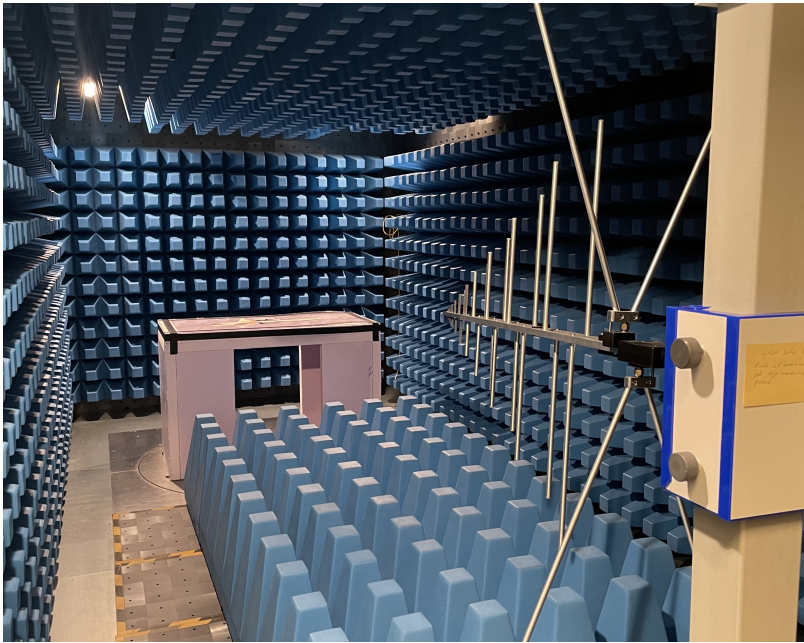


Figure 3.12: The EMC chamber at Axis, which is where all measurements are from. A rotating table at the back, with an BiLog antenna on the right. Attenuating absorbents on the walls to limit reflections.

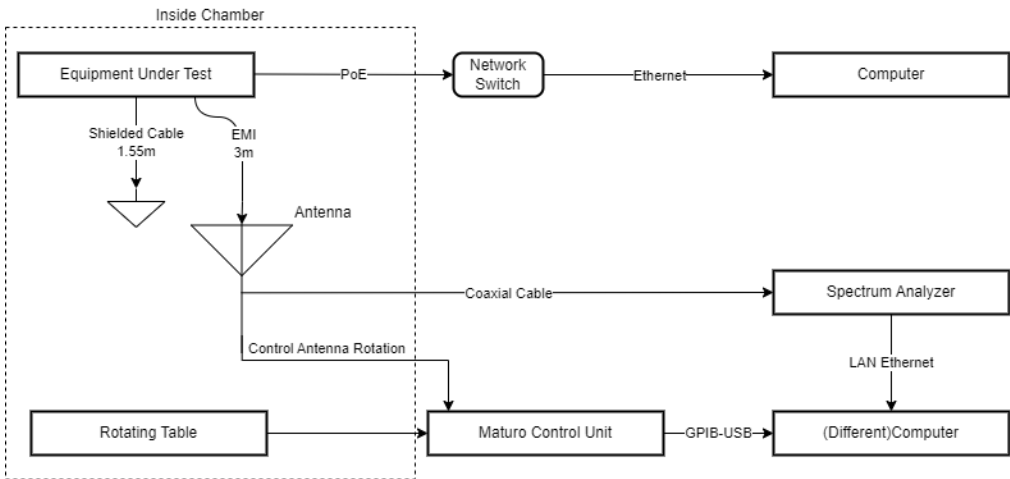


Figure 3.13: Flow chart of the setup for the emission tests.

Standardization of Measurements

In order to get results that are comparable to each other, the tests needed to be standardized. The comb generator that was explained in section 3.2 was placed

inside a metal chassis, which itself was grounded to the EMC chamber ground. This grounding was confirmed using a multimeter and measuring continuity. The specific multimeter used was UNI-T UT33D. This gave the shield a stable ground to connect to, which increased the effectiveness of its electromagnetic emission attenuation. The shield was connected to the chassis using conductive copper tape for the same reason, which was also confirmed using the multimeter. The ground of the comb generator was also connected to the chassis in order to have a common ground with the chassis. The EUT was placed in the same orientation each test, since the radiation could be different at different angles. The uncertainty of the chamber at Axis is unknown, however, when it comes to different certified EMC labs the difference could be as high as 5 or 6 *dB* for radiated emissions tests. After two consecutive measurements at the Axis chamber, where nothing was touched or opened between measurements, the precision should be high. So, doing a comparison at the same chamber would give a low systematic error and, therefore, the shielded and un-shielded measurements were made consecutively.

Similar tests were done on an Axis camera, Axis P3245-LVE. The camera was mounted to point towards the antenna, when the table was angled at 0°. The different prototypes were then mounted on top of the camera. When doing measurements on the camera a few aspects needed to be considered. The PoE and ground cables which connected to the camera act as antennas. This meant that there were emissions that could not be attenuated by the shields. These cables are shielded, but some noise remained. It was, therefore, hard to see exactly what could and could not be attenuated by shielding the dome. To see the effect of the cables with respect to the camera, measurements were made. Three tests were done, firstly an un-shielded camera was tested with and without an extra layer of aluminium foil covering the cables. Secondly, the camera was then completely covered with aluminium foil and using the same cables as the previous test. Lastly, the same test but with an aperture in the foil around the lens so that the camera could see.

The spectrum analyzer in use at the Axis lab is a Rhode & Schwarz ESL6 EMI Test Receiver. It has a frequency range of 9 *kHz* to 6 *GHz* (Rohde & Schwarz 2022). During the measurements, the filter bandwidth was 120 *kHz* for frequencies from 30 *MHz* up to 1 *GHz* and 1 *MHz* when measuring frequencies

from 1 up to 6 GHz , as the EMC standard specifications specify (Swedish Standards Institute 2015). The filter bandwidth uncertainty from the manufacturer is 3% and the magnitude of measurement uncertainty is 0.5 dB for frequencies up to 3 GHz .

The antenna used to collect the radiated interference is a BiLog antenna, this is a combination of a bi-conical and a log periodic antenna. The bi-conical antenna is specified for frequencies in the 30 to 300 MHz range, while the log periodic is specified for measurements between 300 MHz and 1 GHz . This combination of antennas is the most used antenna for radiated emissions in commercial testing and one of the reasons for this is that there is no need to change antenna in the 30 MHz to 1 GHz range (Williams 2017:150). The bilog antenna used in this thesis can be seen in figure 3.14.

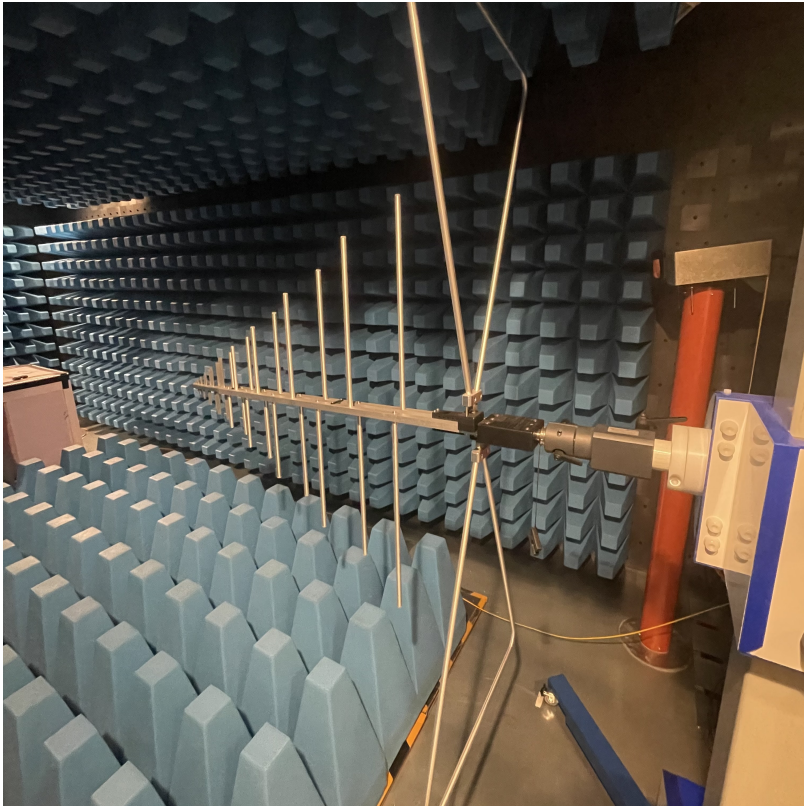


Figure 3.14: BiLog antenna in its vertical position, from Axis EMC chamber. Log periodic part at the front and the biconical at the back.

The frequency range for the tests were between 30 *MHz* and 1 *GHz*. This frequency range is where most radiated emissions tests are measured (Williams 2017:153). At Axis this is also the case for its cameras. The antenna was stationed 3 *m* away from the EUT and both were placed 1.55 *m* above the floor. The EMC standard specifies for radiation emission tests below 1 *GHz*, that the antenna should be 10 *m* from the EUT (Swedish Standards Institute 2015). This cannot be done because of the size limitations of the chamber, instead the emission level limit can be adjusted for a better comparison to the standard. The intensity difference from going from 10 to 3 *m* is 10.45 *dB* higher at 3 *m*, using equation 3.2. Where G is the intensity gain when moving closer to the source, R_1 is the furthest distance and R_2 is the closest distance.

$$G = 20 \cdot \log\left(\frac{R_1}{R_2}\right) [dB] \quad (3.2)$$

During the measurement, the EUT was rotated in 45° steps and the spectrum analyzer sweeps through the spectrum at each angle. This was done with the antenna being in a horizontal as well as a vertical position. This procedure was pre-programmed by Axis. The resulting graph was the EM-field level in *dBμV/m* as a function of the frequency using a logarithmic scale, where each value is the strongest peak at that frequency across all angles. See graphs in Appendix A for a demonstration. Thereafter, the program lets you choose which frequencies to measure with quasi-peak. After choosing the frequencies, the program measures each frequency one by one, with the table moving plus and minus 23° from the previous 45° step. It does this so it can home in on the maximum field emission per frequency. See table figures under column "Azimuth (deg)" in Appendix A for a demonstration of which angles gave the maximum emissions.

For the lower frequencies, the measurements needed to be converted because of the limitations of the chamber. For the standard of radiated emission below 1 *GHz*, it says the antenna must be 10 meters from the EUT. This is not the case for frequencies above 1 *GHz*. The electric field strength E can, as previously mentioned, be defined according to equation 2.6 in section 2.5.3. The equipment in the chamber was, however, already calibrated with the attenuation and antenna factor in mind. Therefore, what was left to measure were the emissions of the EUT. The total field strength was calculated in the computer and was then presented in a graph.

After the spectrum had been measured, and the results presented, some frequencies could be chosen for a more thorough measurement. In this case, the frequencies were chosen based on their relevance in the un-shielded case. The measurement system then zoomed in on these peaks and analysed them again. Finally, a quasi-peak measurement, which was described in section 2.6, was made on the different peaks.

The tests of the emissions from the cables for the camera were different compared to the other emission measurements. Here the table was locked to a specific angle, in this case 0° . The spectrum analyzer then scanned the chosen frequencies and presents a graph. It does this at frequency steps of 40 kHz and it scans for 10 ms per step. These measurements were done in this way because this test has a higher resolution. This setup was recently re-programmed, so it was not an option when doing the other measurements.

3.4.2 Image Quality Measurements

Since the different materials were supposed to be transparent, a few tests on image quality were conducted. These tests were made for comparison of transparency of the different materials. A camera from the AXIS M31 series was used for this analysis, see figure 3.15. This is because it had a flat lens cover, instead of a dome, which simplified the tests and removed possible problems like reflections and having to build proper domes using the materials. Instead, a small, flat piece of a transparent conductive material was fastened to the camera. Moreover, a test on how well infrared, or IR, transmits through the materials was done. Axis cameras use infrared light as well to, among other things, see in dark areas. Even though a material might have great transparency and visibility, it might attenuate the infrared wavelengths too much, removing the possibility of IR vision. For the camera in figure 3.15, the IR LED:s operates at a wavelength of 850 nm .

The setup consisted of a camera, camera mount, computer and a wall full of pictures. The camera was mounted facing the wall, so that all pictures were visible, see figure 3.16. The computer controlled the camera and took a snapshot of the wall. The image could then be viewed and analysed on the computer. Pictures were taken for each material. The material was attached to the screen of the camera, so that the field of view goes through the material completely, see



Figure 3.15: Camera from AXIS M31 dome camera series (Axis Communications AB n.d.).

figure 3.17. It was important to make sure that the material was not bent, which would create reflections, and that it covered both the lens and the IR sensors for the tests. A close up of the wall can be seen in figure 4.24. For the visual light measurements two LED lamps were illuminating the motive, which the camera was focused on. For the IR measurements, all lamps were turned off, except for the two IR LED:s on the camera.

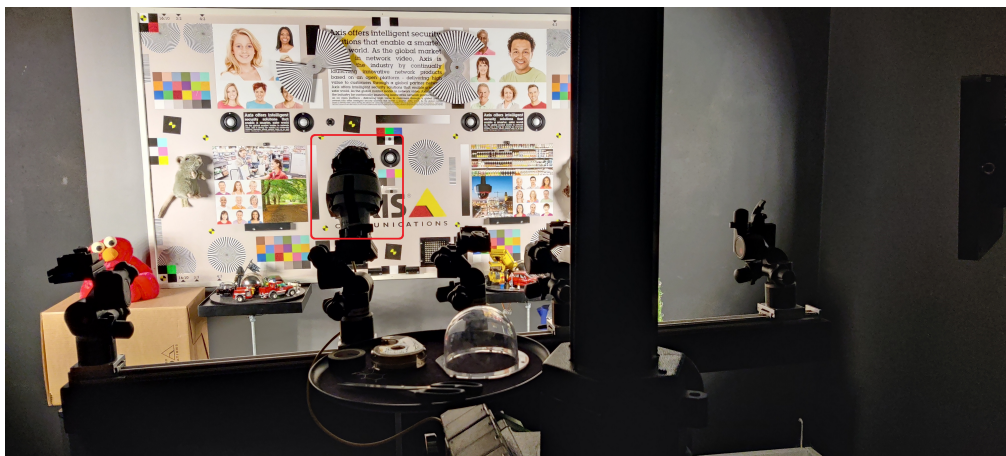


Figure 3.16: Setup of the image quality tests. Camera is pointed towards the wall with some pictures. The camera is highlighted in red.



Figure 3.17: Close up photo on the mounted camera, with the aluminium mesh attached to the lens.

3.5 Analysis and Evaluation

Lastly, an analysis of the results was done. The data from the EMC chamber was imported to Microsoft Excel, where the data could be properly examined. Some graphs were constructed for easy comparisons, which were then analyzed and discussed in this thesis. The different solutions were compared to each other and to the reference measurements. The emission results were then evaluated based on the improvement and to the class A CISPR standard, as described in section 2.6. The image quality was evaluated based on the parameters explained in section 3.4.2. Since the cameras are to be mass produced, the cost of the material is an important factor for the industry. This was evaluated by measuring the paper template maximum length and width in order to get its approximate area and then calculating each material cost per shield with equation 3.3.

$$C [cost/shield] = \frac{P_{material}}{A_{material}} \cdot A_{template} \left[\frac{Price \cdot Area}{Area} \right] \quad (3.3)$$

The material area $A_{material}$ in the equation is the whole area of the product before cutting it to shape. The price $P_{material}$ is the price of each material from the suppliers and the area $A_{template}$ is the paper template used to form the shields. For the liquid PEDOT:PSS and conductive ink which was coated on the domes, the cost per shield was calculated by weighting the material before and after. The prices in the analysis were limited by the suppliers chosen to source the materials from.

4

Results

This chapter presents the results of the cost analysis, measurements from electromagnetic emissions- and image quality tests. A deeper discussion and analysis is made in chapter 5. More EMC tests, such as the whole comb generator spectrum up to 6 GHz, can be found in appendix A.

4.1 Comb Generator

Figure 4.1 shows the waveform going through the antenna and figure 4.2 shows the frequency spectrum of the signal, measured in the near field. The spectrum confirms the 10 MHz signal source, as given by the specifications of the oscillator.

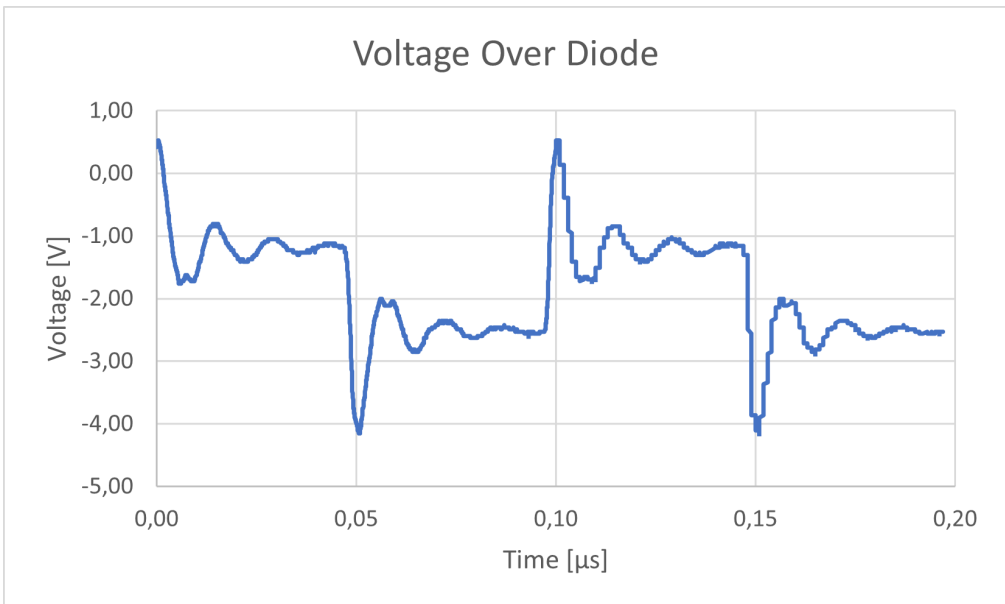
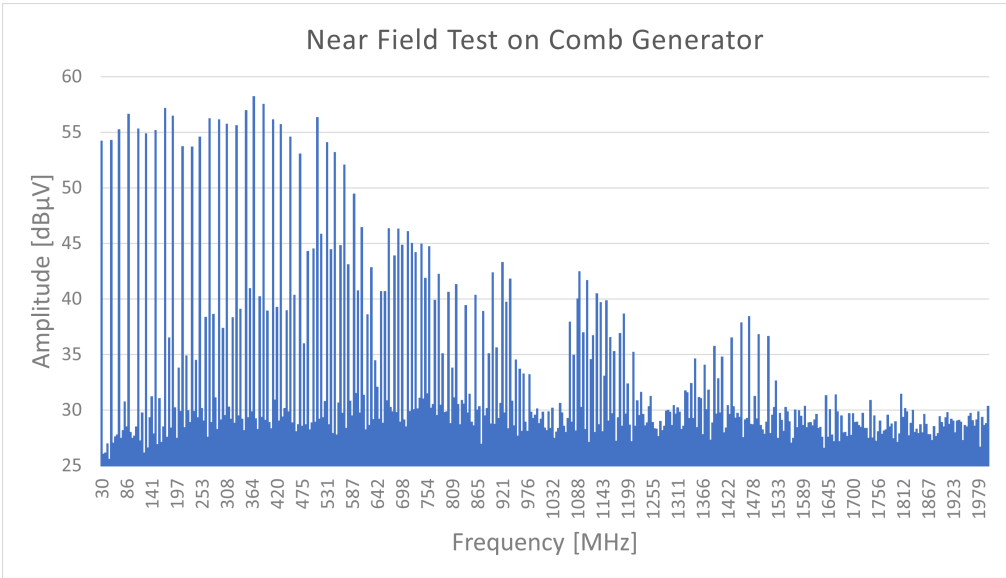
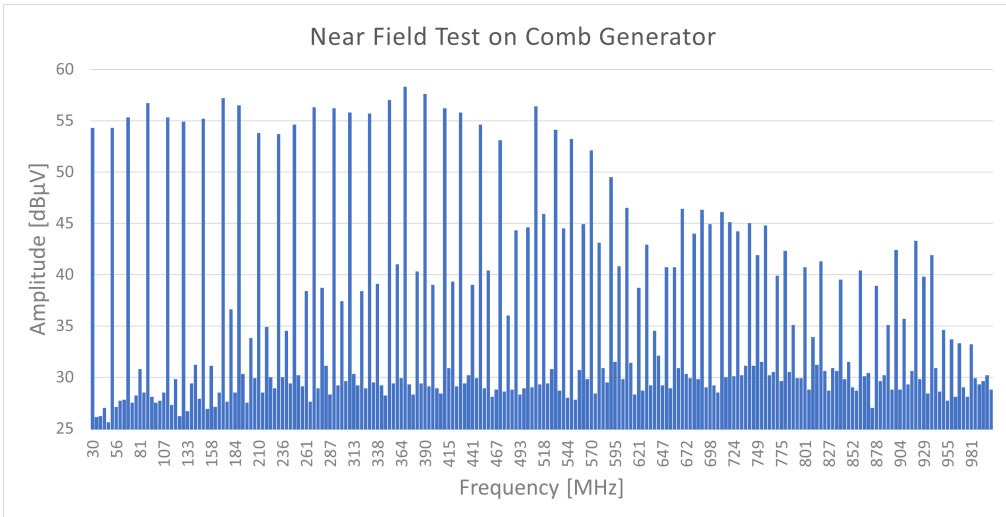


Figure 4.1: The waveform of the output signal, measured by the RIGOL oscilloscope connected between the antenna node and ground.



(a)



(b)

Figure 4.2: The spectrum of the near field signal from the comb generator, using the Keysight spectrum analyzer. (a) From 30 MHz to 2 GHz. (b) From 30 MHz to 1 GHz, here it can be observed that the smaller peaks are not aliasing.

4.2 Emissions From Comb Generator

In this section the various results of the emission measurements are presented, using a comb generator as the noise source. Each material has a resulting graph

of the chosen frequencies, as well as the shielding effectiveness, of the material, as a function of frequency. The theoretical values were calculated using equations 2.3 and 2.4. They also have a near field measurement to see the effects of a given shield in the reactive near field. The real values could be obtained by comparing un-shielded to shielded quasi-peak measurements. The battery voltage was measured between each test to make sure that it was above 7 V, as was required by the regulator. The figures in this section are made in Microsoft Excel, with the goal being easy comparison of peaks at certain frequencies. These frequencies were chosen based on relevance in the un-shielded case. The frequency span between each measurement point increases for the upper part of the spectrum. The reason for this is that the points were chosen on a logarithmic scale. For the full measurement results, see appendix A. All measurements, apart from the near field tests, were made inside the EMC chamber.

4.2.1 No Shielding

A reference measurement was made for the comb generator, which was compared with a shielded measurement. This measurement was re-done a few times to confirm that it was consistent. The margin to the class A limit was from 8 dB above to 23 dB below the limit. Only one of the frequencies measured was above the limit, which was the 8 dB at 30 MHz.

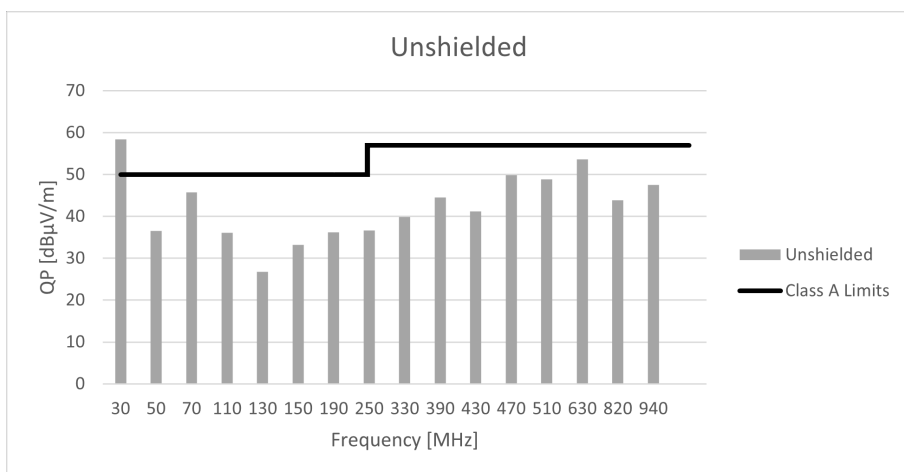


Figure 4.3: Comb generator with no shielding between 30 MHz and 1 GHz.

4.2.2 ITO Film Prototype

The indium tin oxide, ITO, prototype is shown in figure 3.6a, with the results in figure 4.4. The margin to the class A limit is between 14 dB to 39 dB, all below the limit. The graph of the shielding effectiveness can be seen in figure 4.5. The measured shielding effectiveness approximately follows the relationship of the theoretical, that is, a higher effectiveness for the lower frequencies. The near field measurement in figure 4.6 shows that the shield does impact the characteristic using the reactive near field. It is clear that with the shield on, there is attenuation for frequencies above 610 MHz. Then between 200 to 320 MHz and around 590 MHz the shield increases the emissions.

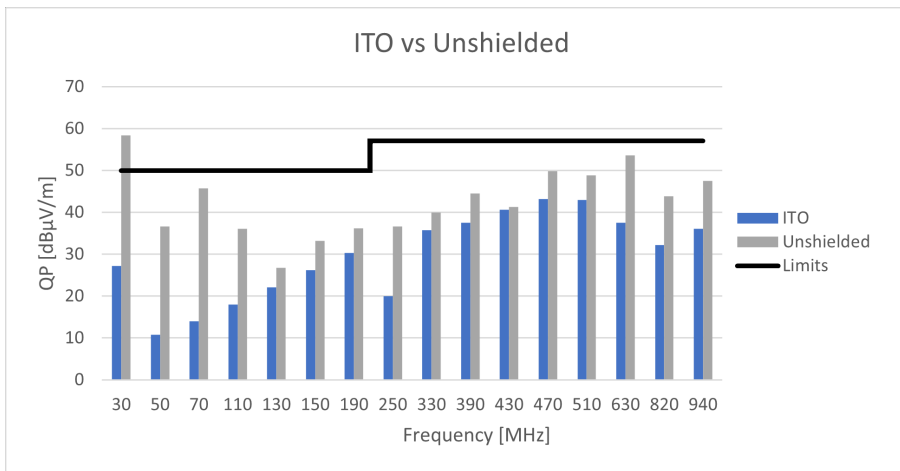


Figure 4.4: Comb generator with ITO shielding between 30 MHz and 1 GHz.

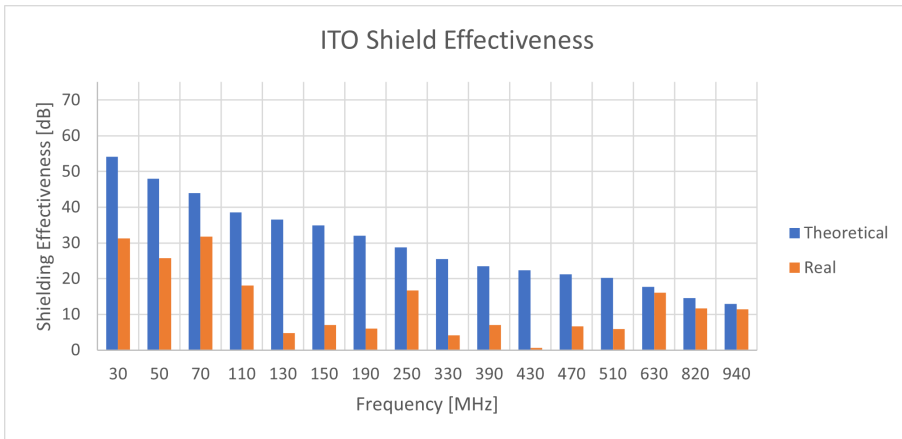


Figure 4.5: Theoretical and measured (Real) shielding effectiveness for the indium tin oxide film.

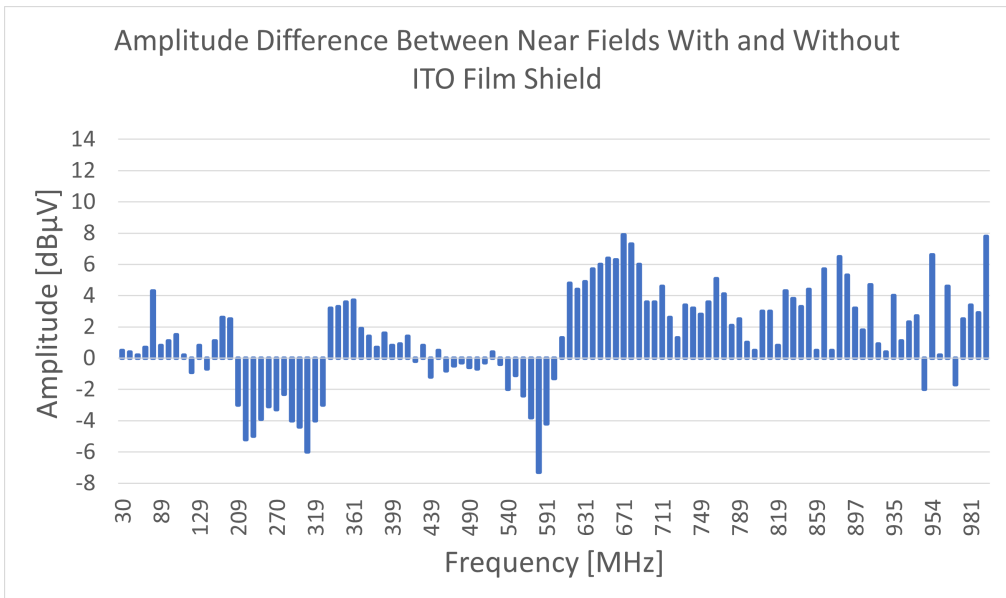


Figure 4.6: Difference in amplitude between near field measurements of comb generator with and without ITO shielding 30 MHz to 1 GHz measured inside the shield. Positive values means that the shield has reduced the amount of emissions. Negative values means that the emissions are increased.

4.2.3 Silver Film Prototype

A transparent film with a silver conducting layer was used for this shield, shown in figure 3.6b. The results show in figure 4.7. The margin to the limit was be-

tween 16 and 47 dB, all below the limit. All emission below 110 MHz were eliminated. The SE graph, figure 4.8, shows a close relationship between the theoretical and the measured effectiveness. In figure 4.9 is the near field measurements before and after adding a shield to the chassis with the comb generator. From 690 to 1000 MHz there is attenuation with the shield on. From 600 to 690 MHz the opposite is true, the shield increased the emissions. For the rest of the frequencies there is not a big enough difference between the two to say if the shield had an impact on the circuit.

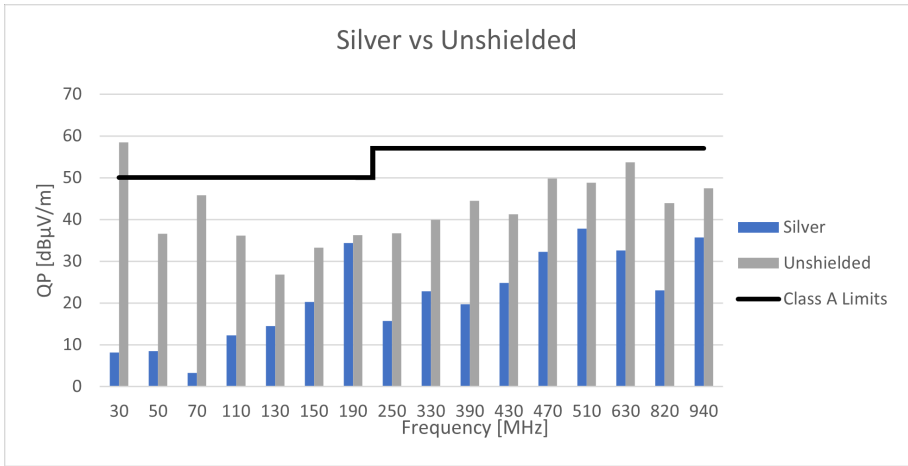


Figure 4.7: Comb generator with silver film between 30 MHz and 1 GHz.

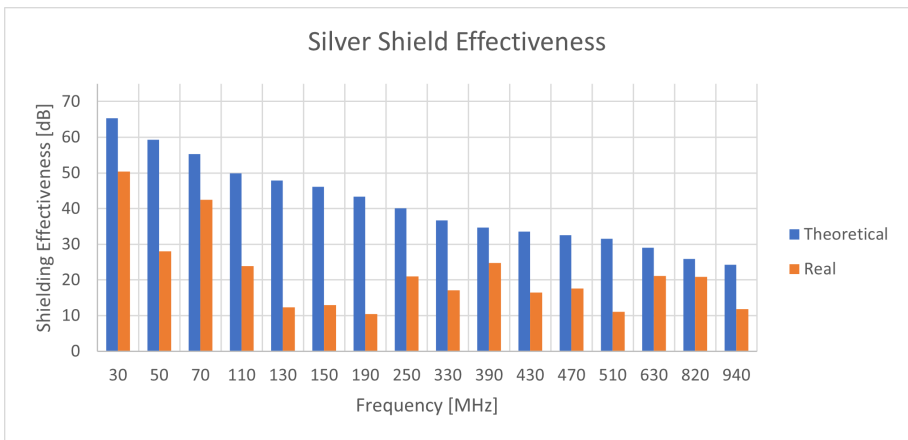


Figure 4.8: Theoretical and measured (Real) shielding effectiveness for the silver film.

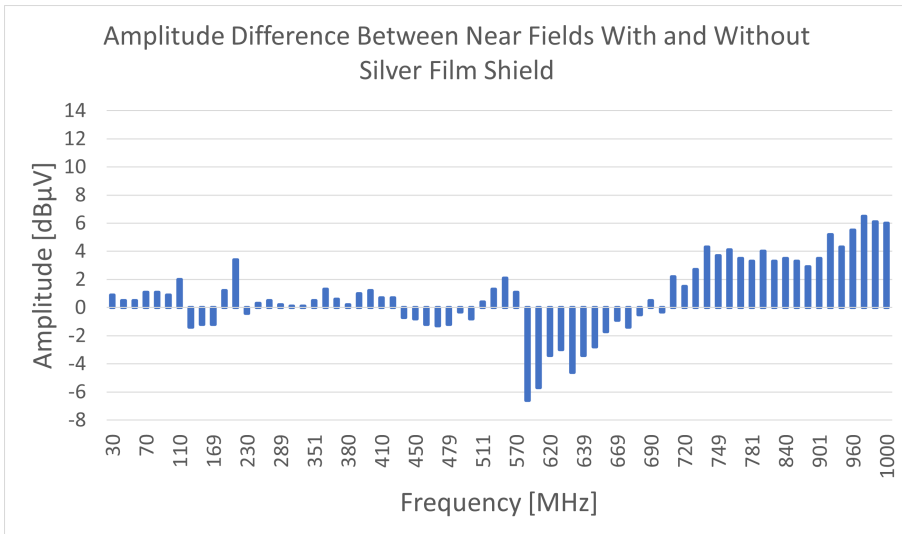


Figure 4.9: Difference in amplitude between near field measurements of comb generator with and without silver shielding 30 MHz to 1 GHz measured inside the shield. Positive values means that the shield has reduced the amount of emissions. Negative values means that the emissions are increased by the shield.

4.2.4 Galvanized Steel Wire Mesh Prototype

For this shield, shown in figure 3.7a, a galvanized mesh was used with an aperture size of 20 mm. The margin to the class A limit was between 6 dB to 38 dB, all below the limit. The SE graph shows a consistent attenuation of emissions across the spectrum. As mentioned in the literature study, the analytical shielding effectiveness for the metal meshes is a very rough approximation. The reactive near fields effect on the emissions does not seem substantial until above 781 MHz and around a frequency of 610 MHz, as can be seen in figure 4.12. Like for the other results so far, the shield attenuates the higher frequencies and increase the emissions in the middle. Outside of these two ranges it looks like the results are within the margin of error from each other.

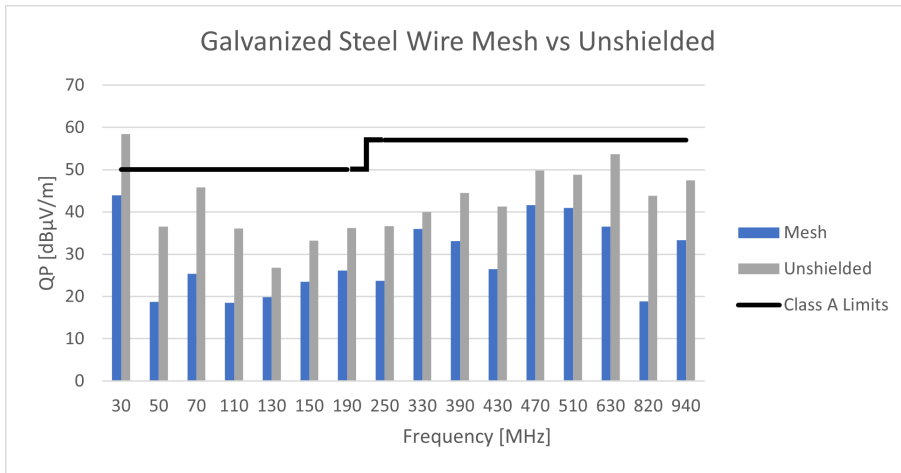


Figure 4.10: Comb generator with galvanized steel mesh below 1 GHz.

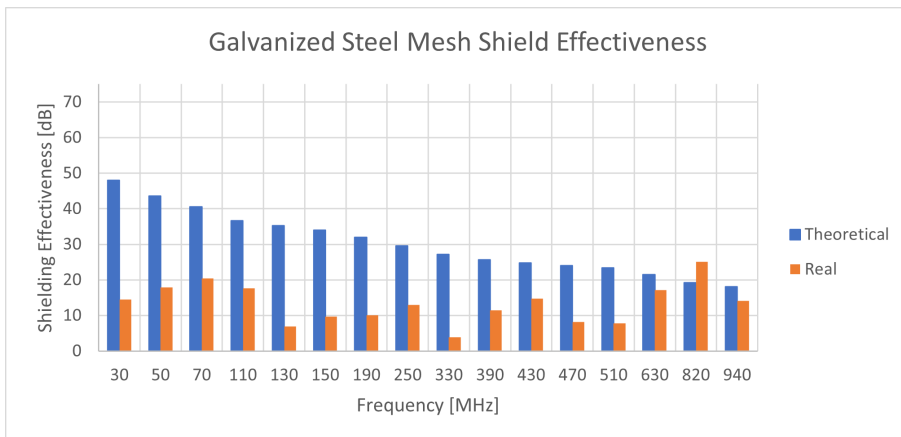


Figure 4.11: Theoretical and measured (Real) shielding effectiveness for the galvanized steel mesh.

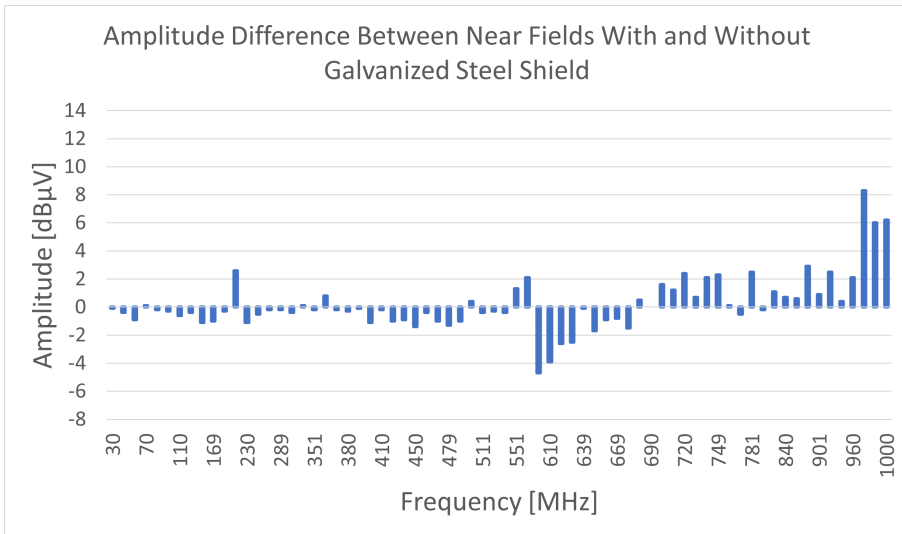


Figure 4.12: Difference in amplitude between near field measurements of comb generator with and without galvanized steel shielding 30 MHz to 1 GHz measured inside the shield. Positive values means that the shield has reduced the amount of emissions. Negative values means that the emissions are increased by the shield.

4.2.5 Aluminium Mesh Prototype

This shield uses an aluminium mesh with a mesh size of 2x3 mm, shown in 3.7b. The margin was between 11 dB to 47 dB, all below the limit. This can be seen in figure 4.13. All emission below 130 MHz were eliminated. There still exist emission at 30 to 110 MHz and this is because that is the noise floor in the chamber. The shielding effectiveness in figure 4.14 shows that the measured SE follows a similar relationship to the theoretical. The effectiveness of the shield in the reactive near field seem to start around 500 MHz. The results of the reactive near field test with and without the shield can be seen in figure 4.15. Here the largest attenuated signal can be seen at 1000 MHz. From 500 to 1000 MHz the emissions are attenuated with the shield present. Around 460, 360, 310 and 160 MHz the emissions are increased with the shield mounted.

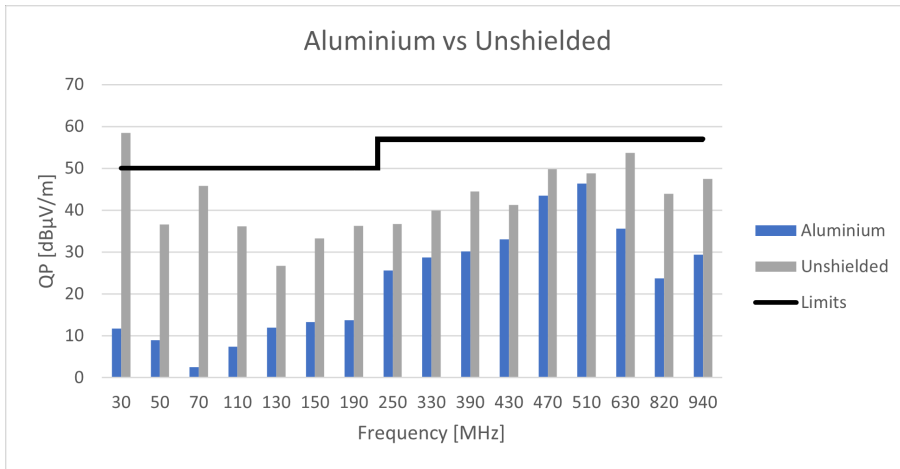


Figure 4.13: Comb generator with aluminium mesh below 1 GHz.

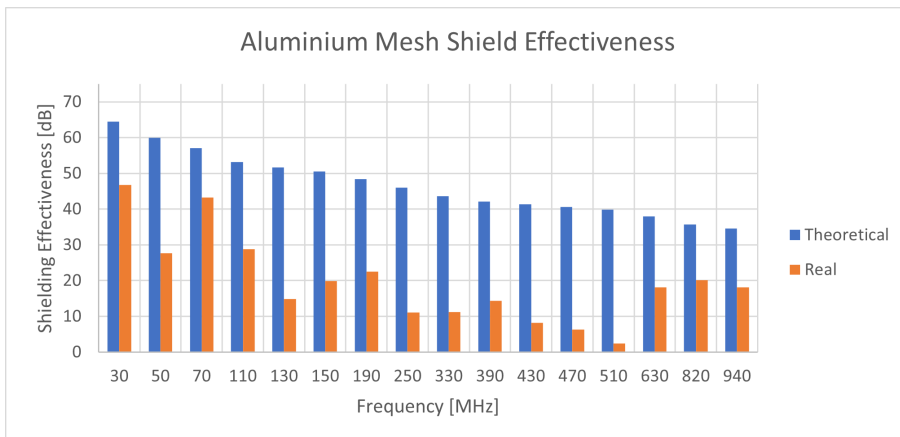


Figure 4.14: Theoretical and measured (Real) shielding effectiveness for the aluminium mesh.

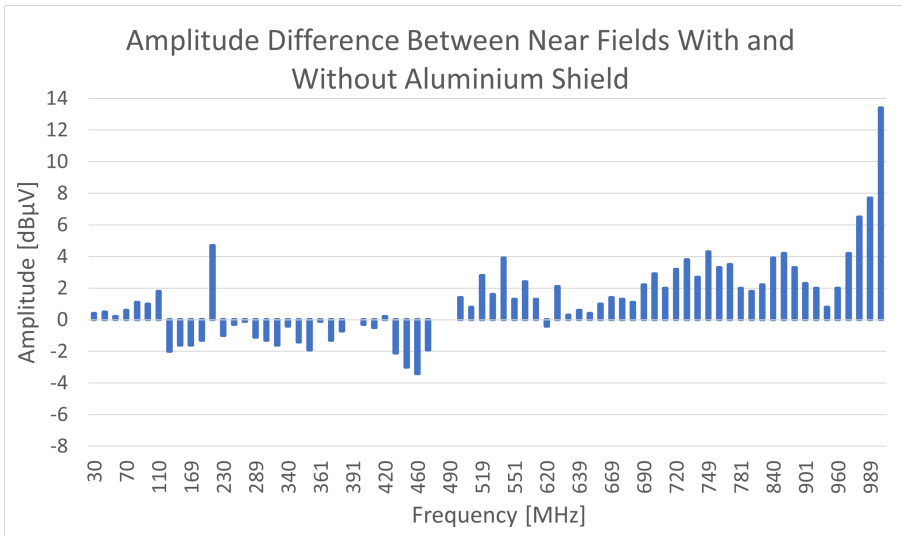


Figure 4.15: Difference in amplitude between near field measurements of comb generator with and without aluminium mesh shielding 30 MHz to 1 GHz measured inside the shield. Positive values means that the shield has reduced the amount of emissions. Negative values means that the emissions are increased by the shield.

4.2.6 Failed Prototypes

Two of the prototypes did not qualify for emission testing. A week after the ink shield were made, cracks started forming on the mesh, thus, making it less and less conductive. This combined with the fact that the material is not transparent, led to the decision to not continue working with it. Also, the PEDOT:PSS could not completely cover the dome, making it impossible to function as a shield. Further investigations are needed for these materials.

4.3 Emissions From the Camera

In this section the various results of the emission measurements, using the P3245-LVE camera as the emission source. Each material has a resulting graph of the chosen frequencies and each shield is compared to an un-shielded camera. All measurements are made with the Rohde & Schwarz spectrum analyzer in the EMC chamber, as described in 3.4.1.

4.3.1 Camera With No Shielding

The reference measurement of the camera yielded the results as follows. As previously explained, some of the lower frequency peaks comes from the cables which are connected to the camera. Thus, they will not be affected that much by any shielding on the camera. For the whole spectrum, see figure C.1 in appendix C.

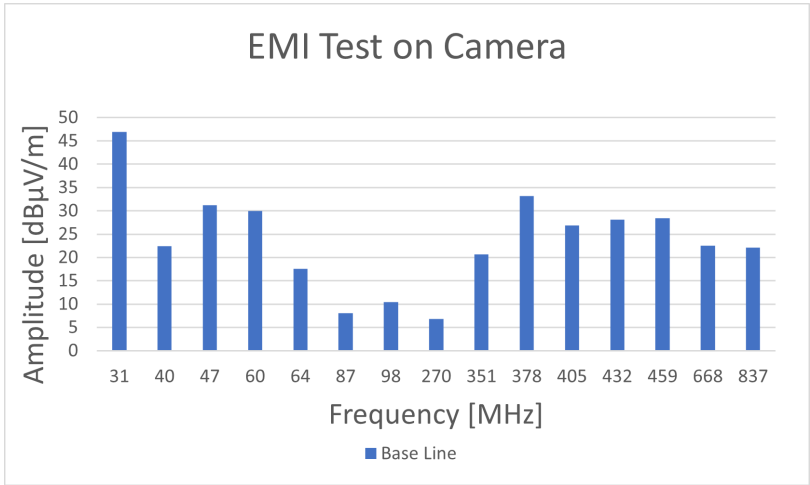


Figure 4.16: Camera with no shield (base line). Measured using quasi-peak that was described in section 2.6

4.3.2 Camera With ITO Film Prototype

The results of using the indium tin oxide prototype, see figure 3.6a, as a shield for a camera. It shows attenuation for peaks at some frequencies. The emissions around 400 MHz managed to be attenuated close to the noise floor, as shown in figure 4.17. Note that some amplitudes are increased when applying a shield. For the whole spectrum, see figure C.2 in appendix C.

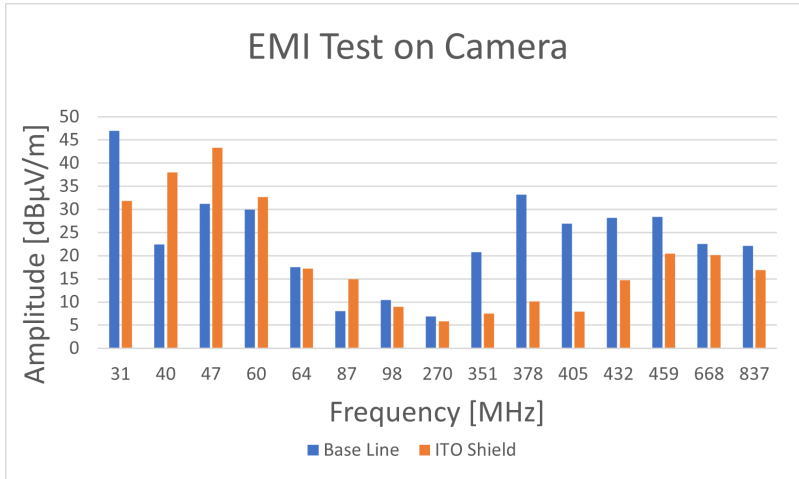


Figure 4.17: Camera shielded with the ITO film and no shield (base line). Measured using quasi-peak that was described in section 2.6.

4.3.3 Camera With Silver Film Prototype

The silver film, figure 3.6b, reduced some of the peaks. The peaks with frequencies around 400 MHz were attenuated to the noise floor, see figure 4.18. Some peaks are increased here as well, such as 64 MHz and 98 MHz. See figure C.3 in appendix C for the whole measurement.

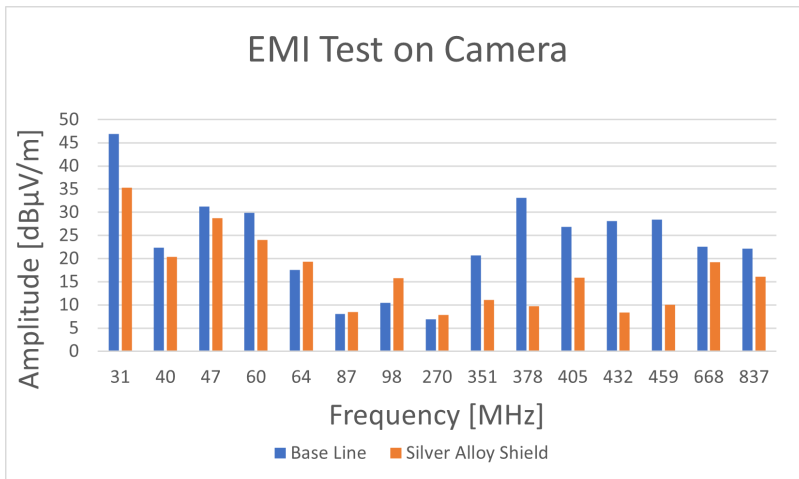


Figure 4.18: Camera shielded with the silver film and no shield (base line). Measured using quasi-peak that was described in section 2.6.

4.3.4 Camera With Galvanized Steel Mesh Prototype

The galvanized steel mesh, figure 3.7a, managed to reduce some frequencies. The frequencies around 400 MHz were slightly attenuated, see figure 4.19. Amplitudes at 64 MHz and 668 MHz are increased. See figure C.4 in appendix C for the whole spectrum.

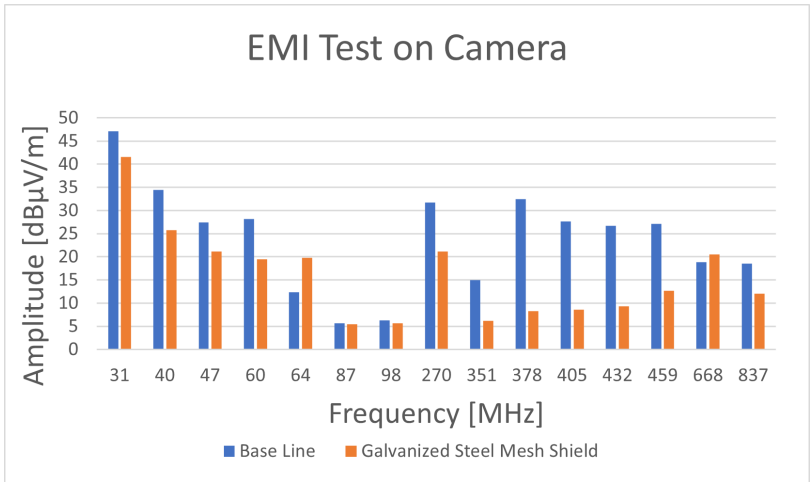


Figure 4.19: Camera shielded with the galvanized steel mesh.

4.3.5 Camera With Aluminium Mesh Prototype

The aluminium mesh, see figure 3.7b, managed to reduce some frequencies. The frequencies around 400 MHz reached the noise floor, see figure 4.20. Peaks at 40 MHz and 87 MHz are increased. See figure C.5 in appendix C for the whole spectrum.

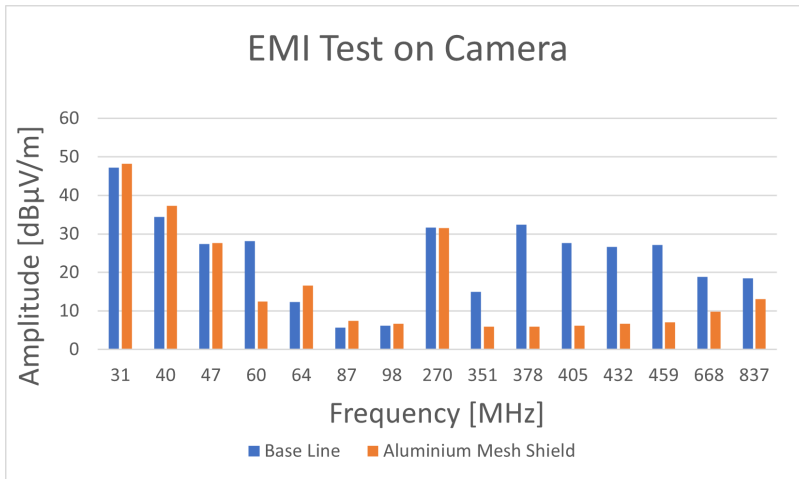


Figure 4.20: Camera shielded with the aluminium mesh.

4.3.6 Camera With an Aperture in the Shield

The purpose of this measurement is to see if an aperture around the camera lens still manages to attenuate emissions and is shown in figure 4.21. The peaks around 400 MHz are attenuated.

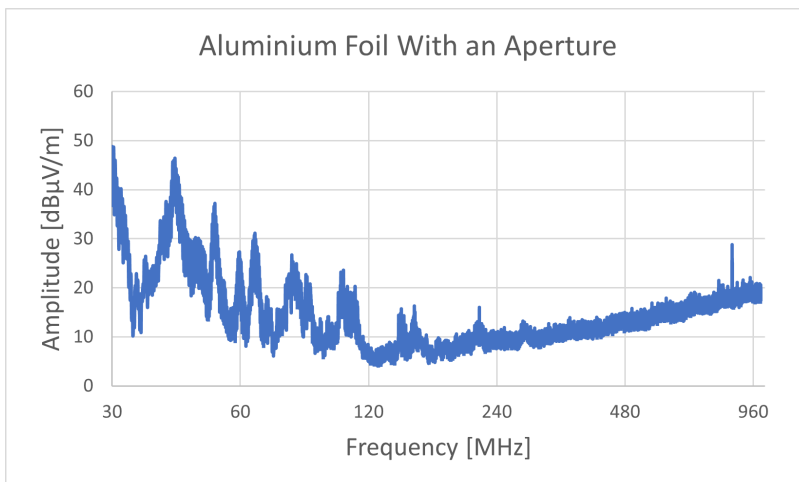


Figure 4.21: Camera shielded with aluminium foil with an aperture over the lens. Continuous scan with 40 kHz steps.

4.3.7 From Cable and Camera

The graphs in this section shows the effect of shielding the PoE cable and an ideal case of shielding, using aluminium foil. These were used for reference and context to the other measurements on the camera. The camera was un-shielded for both lines in figure 4.22 and the PoE cable was shielded and grounded in both cases in figure 4.23.

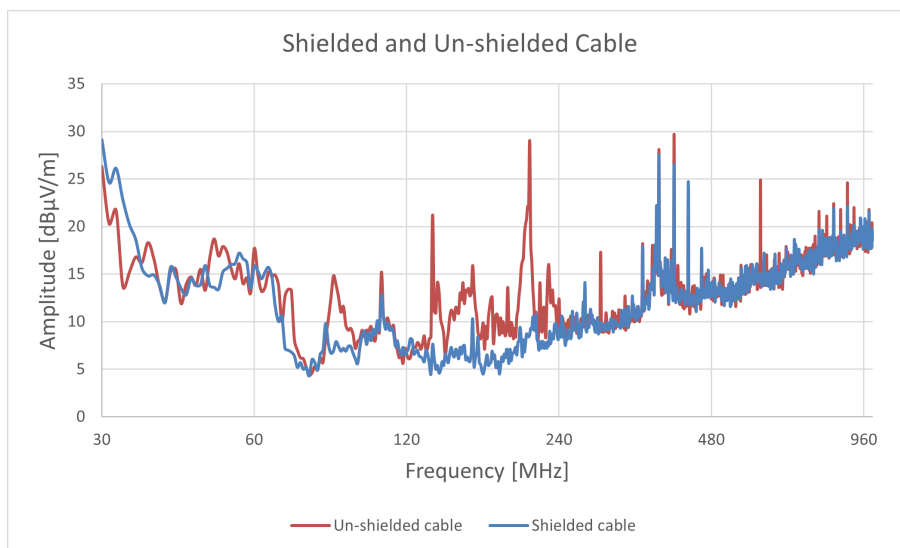


Figure 4.22: Emissions from camera with and without PoE cable shielded. The camera was not shielded.

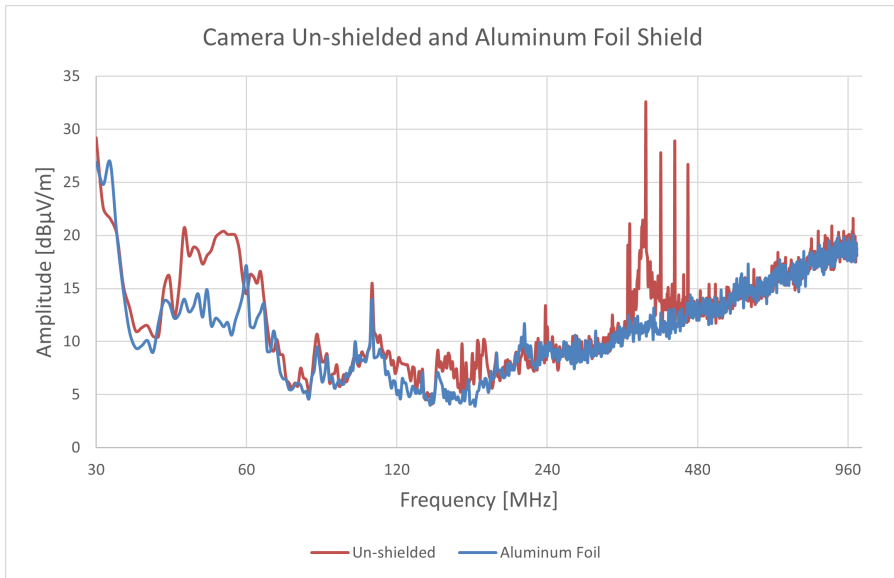


Figure 4.23: The camera is shielded with aluminium foil and un-shielded. With the PoE cable also shielded using aluminium foil.

4.4 Image Quality Tests

This section presents the image quality results of the different prototypes. The format of the displayed quality tests is: first, with no shield present and second, the different materials. This creates an easy comparison between the pictures. Figure 4.24 and 4.25 show the image quality for the different materials. With figure 4.26 and 4.27 showing a zoomed in version of the same snapshot. After the image quality test, the infrared tests are shown in figure 4.28 to 4.31. In Appendix B each image is displayed in its entirety.

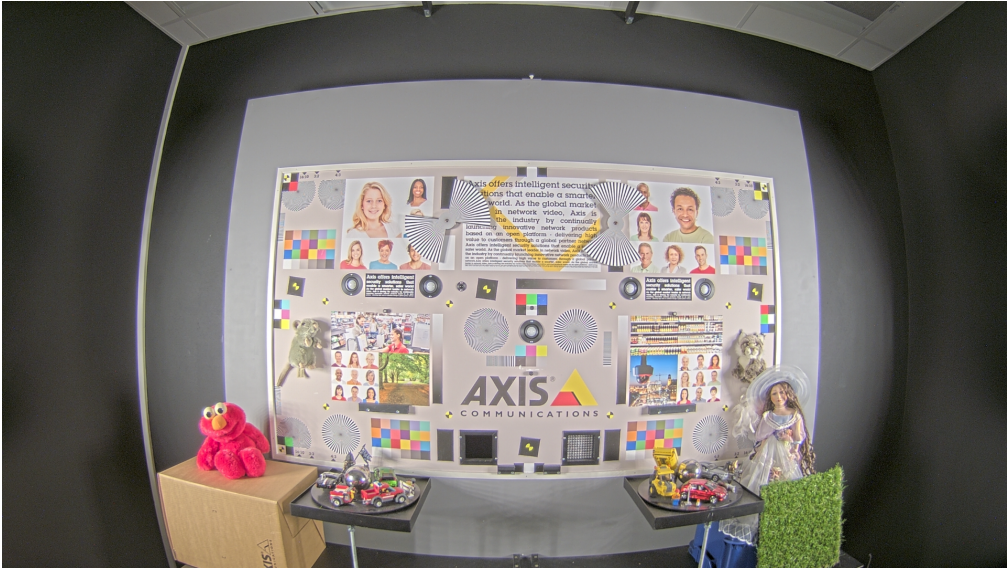


Figure 4.24: Image test with no shield present.

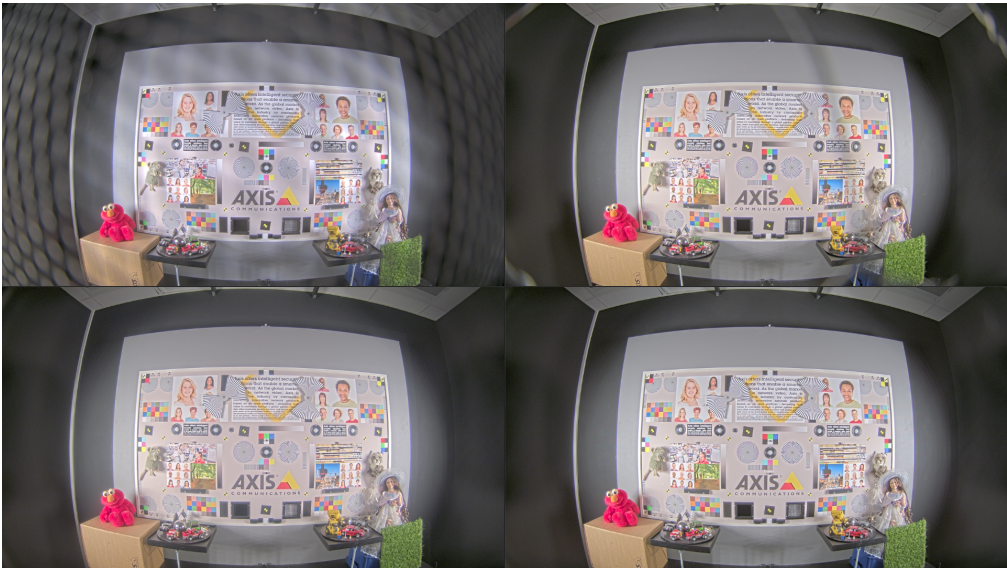


Figure 4.25: Image test with four shields. Starting upper left corner and moving clockwise: aluminium mesh, galvanized mesh, silver film and ITO film.



Figure 4.26: Zoomed in image test with no shield present.



Figure 4.27: Zoomed in image test with four shields. Starting upper left corner and moving clockwise: aluminium mesh, galvanized mesh, silver film and ITO film.



Figure 4.28: IR image test with no shield present.

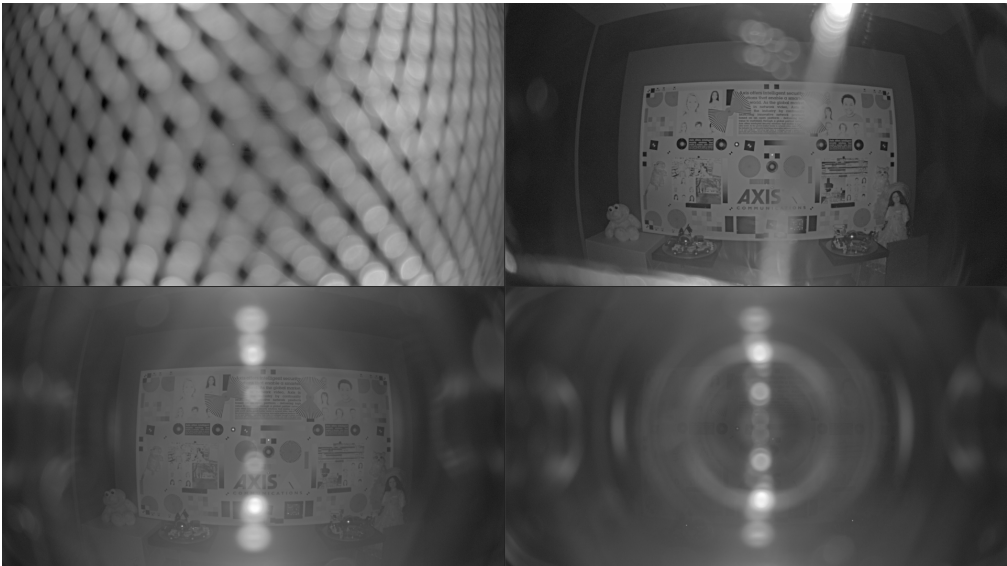


Figure 4.29: IR image test with four shields. Starting upper left corner and moving clockwise: aluminium mesh, galvanized mesh, silver film and ITO film.



Figure 4.30: Zoomed in IR image test with no shield present.

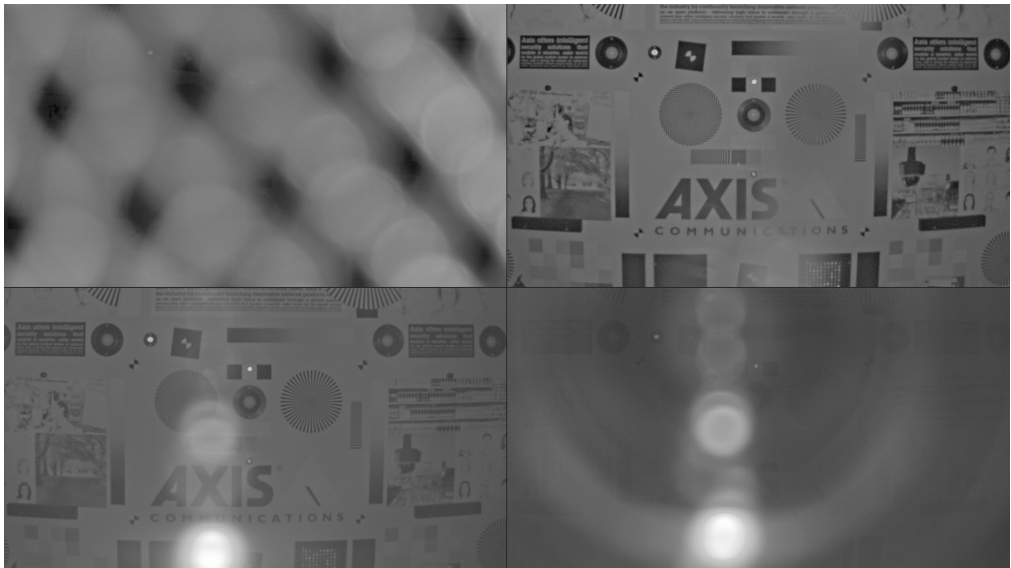


Figure 4.31: Zoomed in IR image test with four shields. Starting upper left corner and moving clockwise: aluminium mesh, galvanized mesh, silver film and ITO film.

4.5 Cost Analysis

The area of the paper template is 297.25 cm^2 , using it with equation 3.3 and with column one to three in table 4.1. The cost per shield can be calculated, which is in column four. For the conductive ink and PEDOT:PSS, their respective costs depends on their weight instead of area. The ink had a weight of 11 grams per tube and the PEDOT bottle contained 5 grams of liquid. To shield a dome with ink, the whole tube was needed. From the supplier website there existed a larger tube with 50 grams of ink, which was used in the calculations for its higher value. For the PEDOT, the supplier had a 25 gram bottle. The best value option from each website will be used in the calculations. Because the polymer failed to stick to the dome, no cost could be determined. The materials in the table 4.1 are sourced from the suppliers in column five.

Table 4.1: Cost table of the materials and where they were sorted from.

MATERIAL	PRICE [kr]	AREA [cm^2]	COST/SHIELD [kr]	SUPPLIER
ITO Film	423	929	135.3	Sigma-Aldrich
Silver Film	289.8	623.7	138.2	DigiKey
Galvanized Mesh	95.2	60 000	0.47	Biltema
Aluminium Mesh	39.2	500	23.3	Biltema
Conductive Ink	469	-	103.2	Electrokit
PEDOT:PSS	2 050	-	-	Sigma-Aldrich

5

Discussion

This chapter contains the reasoning and analysis used to tie this thesis together. At first, the general strategy of the thesis is discussed and evaluated. This is followed by an analysis of the results of EMI reduction, as well as image quality. Finally, a discussion of future development, where some different methods of application of the different materials are discussed, together with important properties not tested in this thesis.

5.1 Strategy and Prototypes

The general strategy used in this thesis was to research possible materials, order components as well as materials. Build prototypes, perform tests and, finally, evaluate the results. This approach was straight forward and made the path clear. This led to a productive working environment and pushed the project forward. The project was performed in the office at Axis, which meant that we went to the office consistently every day. This meant that small increments of progression could consistently be made, and a habit was formed. The habit made it easier to continue working on the thesis and contributed to a good workflow. With the thesis being done at Axis, it was also easy to get tips and guidance whenever needed, which also increased productivity. If a problem occurred, we could quickly get a response from our supervisor at Axis or ask anyone else at the department.

The prototypes were made from the same mould. This gave the tests a standardization which improves comparability between the results. The mould was created so that there were as little overlaps and edges as possible. This was done in order to reduce the points of failure as well as creating a better imitation of how a real application of the material would behave like, that is, a continuous surface. One distinction between these prototypes and a real scenario, is that the prototypes have a conical shape instead of a dome. This could possibly have an

effect of the shields characteristics and how it influences the circuit, especially since it is in the reactive near field for some wavelengths.

The structure of the prototypes had other issues as well. One is that the transparent films and metallic meshes did have some overlap of material on one side of the prototype. This could affect the results into some misleading conclusions. It was important to make sure that the shields had proper connection to the chassis, which was done using copper tape. However, too much tape surface would skew the measurement to perform better than it should. This is because the tape is highly conductive and could create a copper mesh-like shield, which would give misleading results. So, it was also important not to exaggerate the use of copper tape. A better way of prototyping the materials would have been to apply them directly on the dome. But since the surface is curved, it would require custom tools. So, it was decided, due to the time frame, to limit the scope of the thesis and instead have the focus being on easier applications.

As for the two failed prototypes, the conductive ink and PEDOT:PSS polymer, they were difficult to make. The ink is not a good material to use for this purpose since it is weak and cracks very easily. It also had a high resistance compared to the other materials, which further decreases its shielding effectiveness. For the polymer, it could be a good contender as described in the literature study. We could, however, not test it due to the lack of knowledge and equipment in applying the material to the dome.

5.2 Comb Generator

The comb generator managed to produce satisfactory results. The frequency domain plots, that can be seen in figure A.1 in appendix A, shows that the circuit radiates a plethora of frequencies, over the whole spectrum. The peaks are spaced 10 MHz apart from each other, which corresponds to the fundamental frequency. In the near field, in figure 4.2b it looks like there might be some aliasing due to a low sampling rate occurring in the measurement. This is not the case, however. Figure 4.2a shows a measurement, with a frequency span up to 2 GHz . These smaller peaks that look like aliasing are still present, and the analyzer is rated as measuring frequencies up to 7 GHz . The reason for a lower amplitude for the even frequency component is that the oscillator is close to a

50% duty cycle. The time domain signal can be seen in figure 4.1. It was measured at the antenna, using ground as a reference point. It shows an oscillation created by the capacitor. The square wave from the oscillator is still prevalent. This is unlike in the source material where there are some dirac peaks instead (Kenneth 2015:56). This could be due to several different factors, such as the capacitor value, the capacitor material or another diode to speed up the circuit time constant. However, the results, see figure 4.3, were deemed good enough for the task. Therefore, no alternative improvements were explored.

The antenna is short compared to the relevant wavelengths, which makes it less efficient to transmit the signal. As previously stated, it could not be larger because it was limited by the size of the camera dome. Some ways we tried to compensate for this inefficiency was to change the design from a monopole to a dipole antenna. This was done to reduce the need of a ground plane, which would take up much needed space inside the dome. The radiation pattern of a monopole antenna is also more complex and depends on, among other things, the orientation of the ground plane (Antenna Experts 2022).

5.3 Reduction of Electromagnetic Emissions

The main purpose of the thesis was to find solutions of transparent shielding against electromagnetic emissions, thus, the bulk of the time spent testing was used on this section. Each material showed a clear attenuation of the radiated emissions, which shows a proof of concept when solely looking at this aspect. When using a battery as a power source, one must take the decreasing voltage into consideration. This is because the magnitude of the electromagnetic emission was reduced as the battery voltage lowered. Therefore, the results could become misleading if the same battery was used too much. To reduce this risk, the generator voltage was regulated down to 5 V from the 9 V of the battery. This made sure that it was always a constant voltage for the input. This had the advantage of removing one variable to have in consideration when examining the results.

When adding a conductive structure close to the antenna, in its reactive field explained in section 2.2.1, the structure will impact the circuit and potentially its emission. In section 4.2 the graphs of the near field probes with and without

shields are present. Why most of the attenuation with the shield on is in the higher frequencies, or shorter wavelengths, is on its own a bit of a cumbersome question. As seen in, for instance, figure 4.15, the higher frequencies, above 500 MHz , seem to be attenuated a bit when a shield is close to the antenna. According to equation 2.2, the limit of the reactive near field is at roughly 2.5 cm for this frequency. This is reasonable since that is about the distance from the antenna and the prototype shields. This means that the shields might affect the comb generator differently at frequencies higher than 500 MHz . On the camera tests, however, the prototypes are physically further away from the conductive wires and paths in the circuit. This means that the frequencies which are affected in the reactive near field are at higher frequencies in the spectrum, compared to the comb generator.

5.3.1 Emission Results From the Comb Generator

The strongest attenuation was made by the aluminium mesh, see figure 4.13, especially in low to mid ranges of frequencies. This is consistent with the theory, since aluminium has a strong conductivity, see table in Williams (2017:522), and the ratio between aperture size and wire mesh thickness is the lowest. It is closer to a material without apertures in comparison to the galvanized mesh. This does, however, have a disadvantage in that it is harder to see through the aluminium mesh, for more see section 5.4. The mesh is malleable, so it was easy to form it to the correct shape for prototyping. Even though the galvanized mesh had a large aperture size, it still managed to reduce the emissions over the relevant spectrum. As we explained in the literature study, the shortest wavelength, that is in this frequency spectrum, is about 30 cm . Thus, the aperture sizes of the galvanized mesh are considerably smaller and the theory match reality, in this case. Though, this does mean that if one is interested in attenuation of peaks in higher frequencies, meshes like the galvanized one might struggle.

The transparent films, made of silver and ITO, both managed to attenuate the radiation by several dB . The silver film manages to outperform the indium tin oxide. This is, most likely, due to the great properties like conductivity of silver. The films had some malleability, but not as good as the two metal meshes. This led to a difficulty in forming the films to a dome-like shape. This should be easier with direct application using proper tools. Nevertheless, the prototypes

could be constructed and tested.

Overall, the shielding effectiveness graphs look reasonable. They are, however, a little misleading for the lower frequencies. This is because some of the materials, like aluminium mesh and silver film, hit the noise floor. This can be seen in figure A.6 and A.4 in appendix A. Thus, it would never be possible to see a larger attenuation in this EMC chamber, which limits the maximum possible measured shielding effectiveness. A way to combat this, without reconstructing the whole chamber, would be to have an even stronger noise source. This would be able to see more of the potential of the shields. The silver and ITO graphs, figure 4.5 and 4.8, show a close relationship between theoretical and real shield effectiveness for the higher frequencies but not at the lower end of the frequency spectrum. For some of these frequencies, an explanation could be that the signal is hitting the noise floor, which was explained above. The measured shielding effectiveness graphs of the two metallic wire meshes show some resemblance to the analytical solution. As previously mentioned, though, the theoretical effectiveness of the meshes is only an approximation of what it should look like.

An interesting observation from the emission measurements is that there is no consistent angle of maximum emission between tests per frequency. Looking at the results and tables in Appendix A. This shows that there will be uncertainties between tests when changing shields. Therefore, it was important to only change the shield, and not anything else. This was done by fastening the comb generator to the chassis that the camera is mounted on and placing the chassis in the same way according to markings on the table.

5.3.2 Emission Results From the Camera

Parts of the spectrum from the radiated emission coming from the camera seemed unaffected by whether a shield was used or not. This noise remained even after covering the whole camera in aluminium foil and properly grounding it. These emission peaks come from the PoE cable and grounding cable. This was confirmed by the measurements in section 4.3.7, which shows that these peaks were reduced when the cables were shielded, see figure 4.22 and 4.23 in section 4.3.7. These results show that the cables were acting as antennas and have some emissions. As mentioned earlier, these emissions cannot be reduced solely by

shielding the camera. A major part of the noise that can be reduced is around 400 MHz, which most of the different shieldings manage to attenuate fully. The galvanized mesh was a bit worse than the other prototypes, which all managed to reduce the interference to the noise floor. This does show some potential of the materials, when it comes to attenuation of emissions from real products. Since most of the materials managed to attenuate the emissions close the noise floor, it cannot be determined which one of them performed the best in this case. A noisier camera, or other source, or a lower noise floor would be needed for this.

There are some peaks that seem to be amplified, instead of attenuated, when applying a shield. For silver, galvanized steel and aluminium they all have a higher peak at 64 MHz than without using a shield. It is unknown what causes this peak. It could be that it is a resonance frequency between the shield and camera or oscillators from electronics outside that manages to penetrate the EMC chamber. A good way to test this would be to make a measurement just outside the chamber and see the background emissions. However, due to time constraints this was not possible. There are also some peaks at 87 MHz and 98 MHz that are amplified. This amplification is small enough to be considered within the margin of error in some cases, however, other in cases like the silver or ITO film, the amplification is large. This is within the spectrum of FM radio, which might be the reason for these increases. The ITO also have two large peaks in 40 MHz and 47 MHz which has an unknown origin. We did not delve deeper into these peaks as time became a constraint. Nevertheless, more investigations into this are needed to see whether it is the shields that actually increases the emissions at some frequencies.

Emission Results Without Camera Obstruction

Another way of shielding, without affecting the image quality, would be to shield the camera normally, but leaving a hole for the image sensors. In that case the shielding material would not have to be transparent, which would lead to a lot more options for selection. This was tested on an Axis camera which was completely covered in aluminium foil, see figure 4.21. The results look promising, as some of the emission peaks are attenuated. This is reasonable since the galvanized steel mesh managed attenuation as well and that prototype

consists of several holes. The aperture size needed is also small compared to the shortest wavelength in the spectrum relevant to this thesis. This solution would have problems with emissions of higher frequencies due to the aperture. Another problem with this is that heat could build up more under the shield and, thus, creating other problems. More apertures beyond the one around the camera lens would probably be needed for ventilation.

5.4 Image Quality

Image quality is an important factor to consider while evaluating the shielding properties. This is because a shield could block emissions effectively while it has a considerable impact on the camera image quality. Some of Axis' cameras can capture both visible and IR light, therefore, both spectra needed to be evaluated.

5.4.1 Visible Light Images

The difference in image quality between the reference and the two films are indistinguishable. There were, however, noticeable reflections in the films, if they were not completely flat against the camera. This was not a problem for the flat camera panel. It is, however, unknown if the problem would persist if the conductive layer was directly deposited on the dome. For the two metal meshes, they are noticeable in the full view of the camera, and it is distracting for the viewer. In its zoomed in view, it is quite hard to notice any of the mesh lines. The information covered by the lines is not lost, it is instead similar to being shaded by an object outside the cameras point of view, i.e., it looks darker. The closer the metal meshes are to the lens, more transparent they appear.

5.4.2 Infrared Light Images

None of the images from the IR test are passable in our opinion. The best one of the shields is the galvanized mesh, because of its large aperture size. In its zoomed in view, the image information behind the mesh is blurred. The galvanized mesh is not centered with the hole in the middle of the sensor, for the reason of a worst-case test. If the hole was centered and big enough for it to be

not seen on the camera feed, it would be a viable choice for both image quality and EMC. The ITO prototype has some transparency for IR light, but clear reflections can be seen.

One of the reasons for the low performance of the IR test for the two films and the aluminium mesh, is that they cover the IR LEDs from the camera. For the films it leads to reflections and for the mesh it limits the amount of light passing through and reflects back towards the camera. A solution would be to not let the material cover the infrared diodes, which was discussed in section 5.3.2, or have the IR LED outside of the camera. This result does create the need for some apertures in the shield, though, the result of the galvanized mesh and camera without obstruction indicates that this would be possible while keeping the emissions somewhat attenuated.

5.5 Cost Analysis

From the perspective of the industry the choice of materials is partly based on the lowest material cost. With this stated, some of these prices are higher than if they were bought in bulk order. Specifically, from the supplier Sigma-Aldrich, attempts were made to contact the supplier, to get a better estimation of the cost. But the lowest price they offered was the same as we bought it for. No cost could be calculated for the conductive polymer, as there was no successful shield made to determine it. The costs of the different shields are similar to each other, with the exception of the galvanized steel mesh being an outlier. This had to do with the amount of material we got, its cost per area unit was a hundred-fold higher than the rest. These prices, both absolute and relative to each other, might change when using them on real products. This is because this analysis does not take mass production and price of custom tooling into account.

5.6 Future Development

This thesis has focused on different solutions to transparent shielding of a fixed dome camera. Even though some promising results has been shown, further development is needed before the materials can be used on cameras. One area of improvement is finding, or developing, materials which is transparent for

both visible- and infrared light. Some alternatives could be carbon nanotubes or graphene, both of which has good a transmittance in both spectra (Park et al. 2020; Zheng and Kim 2015:67-68). A major focus of future development, and thus when choosing material, should be on the application method. Several manufacturers of different materials were questioned whether they could apply the material on top of a dome structure. This seemed to be difficult since custom tools are required and the material properties might change when distorted, due to the bent surface. Tests on how the material keeps heat in and out should also be done. Since some materials might act as a thermos, the camera might become too hot and, thus, risking damage.

There are other material properties which might be relevant to investigate as well. One obvious property is how durable the material is. Can it withstand different weather conditions and impacts? This is a crucial characteristic since the cameras need to live up to a standard in order to ensure quality. Another interesting attribute is whether the material could be used as a heating element. If so, anti-fog and general heating could be implemented into the cameras which would improve performance in foggy and cold areas.

6

Conclusions

The results of the Master Thesis shows that some of the materials presented can be used as shields to reduce the electromagnetic emissions across 30-1000 *MHz*. This indicates that, purely from the perspective of reducing electromagnetic emissions, they have a potential of being used for shielding surveillance cameras. For the emissions coming from the comb generator, the shields with the greatest attenuation is in following order:

- Silver film
- Aluminium mesh
- Galvanized steel mesh
- ITO film

This is evaluated from the shielding effectiveness data. With this said all of the shields worked above expectations on shielding. The order of which prototype is the best for reducing emissions from the camera is harder to determine. The two transparent films and the aluminium mesh managed to eliminate emissions at some specific frequencies. In addition to the noise from the camera some noise was emitted from the PoE cable, which affected the total noise levels. Some frequency peaks got an amplitude increase from adding a shield to the camera, we chose to limit our work and not investigate this further because of time constraints.

Since all materials showed potential as shields the cost becomes a more important factor to the choice of material. From the cost perspective we see that the galvanized steel mesh has good value for its attenuation. Then the aluminium mesh and lastly the two films at a combined third place.

The two films had the best transparency for visible light, while the two metallic meshes had worse visibility. The image tests were using a flat faced camera. Thus, it is unknown how the visibility changes for dome-like surfaces

and more research is needed. The aluminium mesh and the silver film were the worst in the infrared light scenario. The two LEDs were blocked by the mesh and was reflected and absorbed by the silver film. As for the galvanized steel and ITO film, they were better but not perfect. There were reflections in the film that made artifacts for the camera. But the light could pass though the material, making it somewhat usable. The galvanized steel was even worse than the visual light test, but more usable than the rest. If the aperture was larger it would not have been notice at all. With this stated, either other materials need to be researched or there needs to be apertures around the infrared transmitter and receiver. A proof of concept for an aperture around the sensors was done and it shows that it should be possible to achieve.

For implementing a shield in the Axis fixed dome cameras, it is our opinion that the way forward is more investigations in applying a transparent coating on the dome. Working with a coating company to find solution to applying a coat to a spherical dome. More materials, for instance, graphene and carbon nanotubes, could also be researched for better IR transparency.

References

Antenna Experts (2022), ‘Difference between Dipole Antenna and Monopole Antenna’. **URL:** <https://www.antennaexperts.co/blog/difference-between-dipole-antenna-and-monopole-antenna>
Accessed on 05/05/2023.

Axis Communications AB (n.d.), ‘Axis m31 dome camera series’.
URL: <https://www.axis.com/products/axis-m31-series>
Accessed on 04/05/2023.

Barr, M. (2001), ‘Introduction to pulse width modulation (pwm)’.
URL: <https://barrgroup.com/Embedded-Systems/How-To/PWM-Pulse-Width-Modulation>.

Bevelacqua, P. J. (2022), ‘Field regions’.
URL: <https://www.antenna-theory.com/basics/fieldRegions.php>
Accessed on 04/05/2023.

Chandler, D. L. (2015), ‘Explained: chemical vapor deposition’. **URL:** <https://www.antennaexperts.co/blog/difference-between-dipole-antenna-and-monopole-antenna>
Accessed on 05/05/2023.

Duffy, A., Zhang, G., Koziel, S. and Wang, L. (2015), ‘Objective selection of minimum acceptable mesh refinement for emc simulations’, *IEEE Transactions on Electromagnetic Compatibility* **57**, 1–4.

Erickson, R. W. and Maksimović, D. (2007), *Fundamentals of Power Electronics*, second edn, Springer. ISBN: 978-0-306-48048-5.

European Commission (2014), ‘Electromagnetic compatibility (EMC) directive’.
URL: <https://single-market-economy.ec.europa.eu/sectors/electrical-and-electronic-engineering-industries->

eei/electromagnetic-compatibility-emc-directive

Accessed on 04/05/2023.

European Commission (2020), 'Critical raw materials resilience: Charting a path towards greater security and sustainability', *COM 2020*.

URL: <https://eur-lex.europa.eu/legal-content/EN/TXT/HTML/?uri=CELEX:52020DC0474>

Accessed on 04/05/2023.

Fakirov, S. (2016), *Nano-size Polymers*, Springer Cham. ISBN: 978-3-319-39715-3.

Fenical, G. (n.d.), 'Rule-of-thumb for calculating aperture size'.

URL: <http://cdn.lairdtech.com/home/brandworld/files/EMI%20Rule-of-Thumb%20for%20Calculating%20Aperture%20Size%20Technical%20Note%20Download.pdf>

Accessed on 04/05/2023.

Hambley, A. R. (2014), *Electrical Engineering: Principles and Applications*, sixth edn, Pearson. ISBN: 978-0-273-79325-0.

Kaliyaraj Selva Kumar, A., Zhang, Y., Li, D. and Compton, R. G. (2020), 'A mini-review: How reliable is the drop casting technique?', *Electrochemistry Communications* **121**, 106867.

URL: <https://www.sciencedirect.com/science/article/pii/S1388248120302186>

Kenneth, W. (2015), 'Harmonic comb generators are useful tools'.

URL: <https://interferencetechnology.com/wp-content/uploads/2015/02/WyattArticle.pdf>

Accessed on 04/05/2023.

Liang, Y., Wen, K., Wu, Z., Pan, J., Liu, W., Yao, L., Liu, P. and Huang, X. (2022), 'Metal mesh-based infrared transparent electromagnetic shielding windows with balanced shielding properties over a wide frequency range'.

Mardiguian, M., Sweeney, D. L. and Swanberg, R. (2017), *Controlling Radiated Emissions by Design*, third edn, Springer. ISBN: 978-3-319-04771-3.

Maurya, S. K., Galvan, H. R., Gautam, G. and Xu, X. (2022), 'Recent progress in transparent conductive materials for photovoltaics', *Energies* **15**(22).

URL: <https://doi.org/10.3390/en15228698>.

Paez B., E., Tremola, C., Azpurua, M., D, R. and Del Pino, P. (2012), 'Theoretical and practical validation tests for a near-field to far-field transformation algorithm using spherical wave expansion', *Revista Técnica de Ingeniería de la Universidad del Zulia* **35**, 109–118.

Park, J., Rho, H., Cha, A., Bae, H., Lee, S. H., Ryu, S., Jeong, T. and Ha, J. (2020), 'Transparent carbon nanotube web structures with ni-pd nanoparticles for electromagnetic interference (emi) shielding of advanced display devices', *Applied Surface Science Elsevier*.

URL: <https://doi.org/10.1016/j.apsusc.2020.145745>.

Rohde & Schwarz (2022), 'Emi test receiver specifications'.

URL: https://scdn.rohde-schwarz.com/ur/pws/dl_downloads/dl_common_library/dl_brochures_and_datasheets/pdf_1/ESL_dat-sw_en_5214-0430-22_v0300.pdf

Accessed on 09/05/2023.

Sveriges Geologiska Undersökning (2020), 'Indium'.

URL: <https://www.sgu.se/mineralnaring/kritiska-ravaror/indium/>

Accessed on 30/05/2023.

Swedish Standards Institute (2007), 'Electromagnetic compatibility (emc) - part 6-3: Generic standards - emission standard for residential, commercial and light-industrial environments (SS-EN 61000-6-3)'. Svenska institutet för standarder.

URL: <https://www-sis-se.ludwig.lub.lu.se/produkter/telecom/elektromagnetiska-storningar-och-elektromagnetisk-kompatibilitet-emc/utsandning/ssen6100063/>

Accessed on 04/05/2023.

Swedish Standards Institute (2015), 'Electromagnetic compatibility of multimedia equipment-emission requirements (SS-EN 55032)'. Svenska institutet

för standarder.

URL: <https://www.sis.se/produkter/telecom/elektromagnetiska-storningar-och-elektromagnetisk-kompatibilitet-emc/utsandning/ssen55032/>

Accessed on 04/05/2023.

Taherian, R. and Kausar, A. (2019), *Electrical Conductivity in Polymer-Based Composites: Experiments, Modelling and Applications*, Elsevier. ISBN: 978-0-12-812541-0.

Texas Instruments (1999), 'LM2576xx Series SIMPLE SWITCHER® Power Converter 3-A Step-Down Voltage Regulator'. **URL:** <https://www.ti.com/lit/ds/symlink/lm2576.pdf?ts=1685436167899>

Accessed on 30/05/2023.

Urper, O., Çakmak, İ. and Karatepe, N. (2017), 'Fabrication of carbon nanotube transparent conductive films by vacuum filtration method', *Material Letters Elsevier*.

URL: <https://doi.org/10.1016/j.matlet.2018.03.184>.

Visser, H. J. (2012), *Antenna Theory and Applications*, John Wiley & Sons Ltd. 9781119990253.

Williams, T. (2017), *EMC for Product Designers*, fifth edn, Elsevier. ISBN: 978-0-08-101016-7.

Xia, Y. and Dai, S. (2021), 'Review on applications of pedots and pedot:pss in perovskite solar cells'.

URL: <https://doi.org/10.1007/s10854-020-03473-wf>.

Zhang, P., Wyman, I., Hu, J., Lin, S., Zhong, Z., Tu, Y., Huang, Z. and Wei, Y. (2017), 'Silver nanowires: Synthesis technologies, growth mechanism and multifunctional applications', *Materials Science and Engineering: B* **223**, 1–23.

URL: <https://doi.org/10.1016/j.mseb.2017.05.002>.

Zheng, Q. and Kim, J. (2015), *Graphene for Transparent Conductors*, Springer. ISBN: 978-1-4939-2768-5.

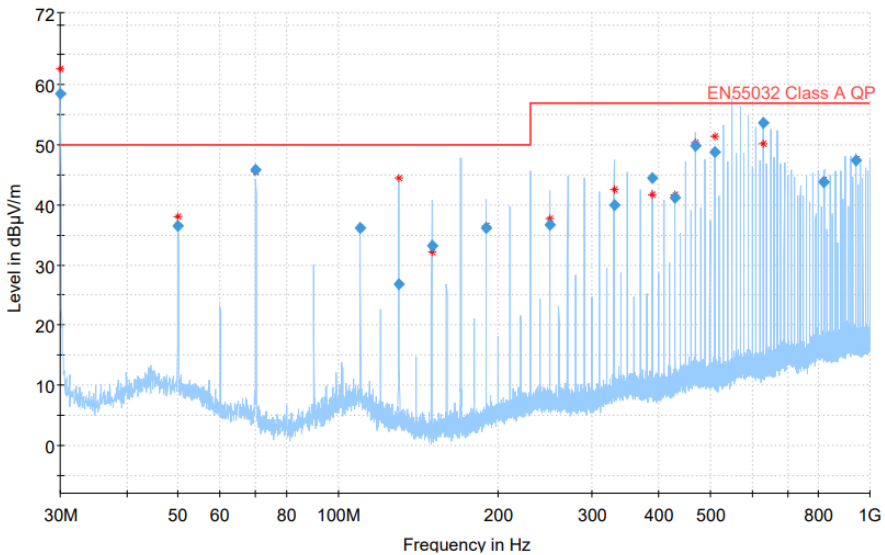
Zhou, J. and Lubineau, G. (2013), 'Improving electrical conductivity in polycarbonate nanocomposites using highly conductive pedot/pss coated mwcnts', *ACS Applied Materials & Interfaces* **5**(13), 6189–6200. PMID: 23758203.
URL: <https://doi.org/10.1021/am4011622>.

7

Appendices

A Comb Generator Emission Graphs

A.1 Without a Shield



Frequency (MHz)	QuasiPeak (dBµV/m)	Limit (dBµV/m)	Margin (dB)	Meas. Time (ms)	Bandwidth (kHz)	Height (cm)	Pol	Azimuth (deg)	Corr. (dB)	Comment
30.003000	58.41	50.00	-8.41	1000.0	120.000	155.0	V	325.0	-15.0	13:37:58 - 2023-05-03
50.000245	36.58	50.00	13.42	1000.0	120.000	155.0	V	294.0	-12.9	13:38:40 - 2023-05-03
69.997289	45.77	50.00	4.23	1000.0	120.000	155.0	V	-20.0	-17.3	13:30:53 - 2023-05-03
110.000178	36.12	50.00	13.88	1000.0	120.000	155.0	H	128.0	-15.4	13:34:46 - 2023-05-03
129.996556	26.75	50.00	23.25	1000.0	120.000	155.0	H	114.0	-18.3	13:35:24 - 2023-05-03
149.998956	33.21	50.00	16.79	1000.0	120.000	155.0	V	336.0	-18.6	13:39:06 - 2023-05-03
189.992244	36.22	50.00	13.78	1000.0	120.000	155.0	V	332.0	-16.0	13:39:42 - 2023-05-03
249.996311	36.67	57.00	20.33	1000.0	120.000	155.0	V	114.0	-13.8	13:36:08 - 2023-05-03
329.993444	39.91	57.00	17.09	1000.0	120.000	155.0	V	85.0	-11.9	13:33:29 - 2023-05-03
389.992978	44.51	57.00	12.49	1000.0	120.000	155.0	V	22.0	-10.7	13:31:16 - 2023-05-03
429.990422	41.23	57.00	15.77	1000.0	120.000	155.0	H	184.0	-10.0	13:36:54 - 2023-05-03
469.989178	49.84	57.00	7.16	1000.0	120.000	155.0	V	94.0	-9.3	13:34:03 - 2023-05-03
509.990066	48.82	57.00	8.18	1000.0	120.000	155.0	V	292.0	-8.5	13:37:32 - 2023-05-03
629.983956	53.63	57.00	3.37	1000.0	120.000	155.0	V	13.0	-6.4	13:31:51 - 2023-05-03
819.976978	43.86	57.00	13.14	1000.0	120.000	155.0	V	-22.0	-3.4	13:32:32 - 2023-05-03
939.976734	47.46	57.00	9.54	1000.0	120.000	155.0	V	22.0	-1.9	13:32:51 - 2023-05-03

Figure A.1: Comb generator with no shielding from 30 MHz to 1 GHz. In the table, **Pol** means whether the antenna is angled vertically or horizontally.

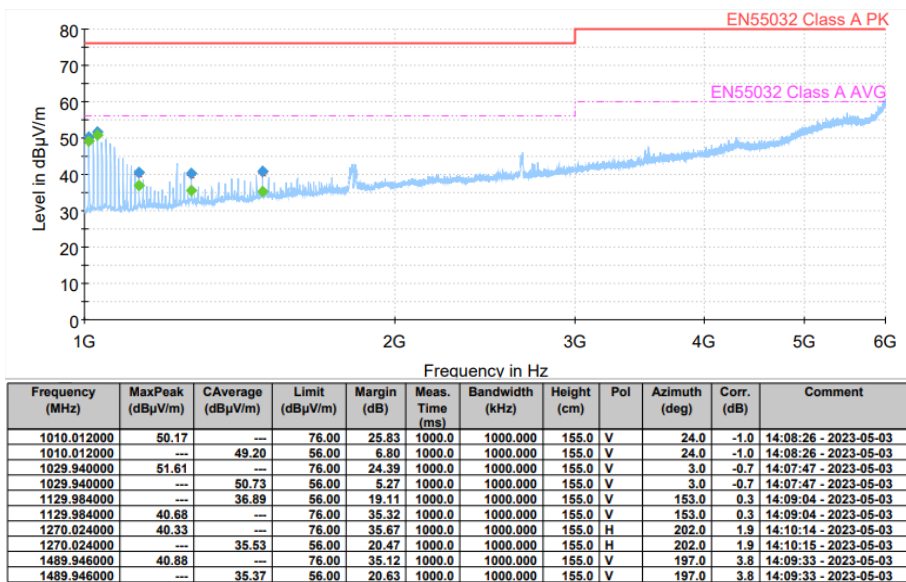


Figure A.2: Comb generator with no shielding from 1 GHz to 6 GHz. In the table, **Pol** means whether the antenna is angled vertically or horizontally.

A.2 With an ITO Film Shield

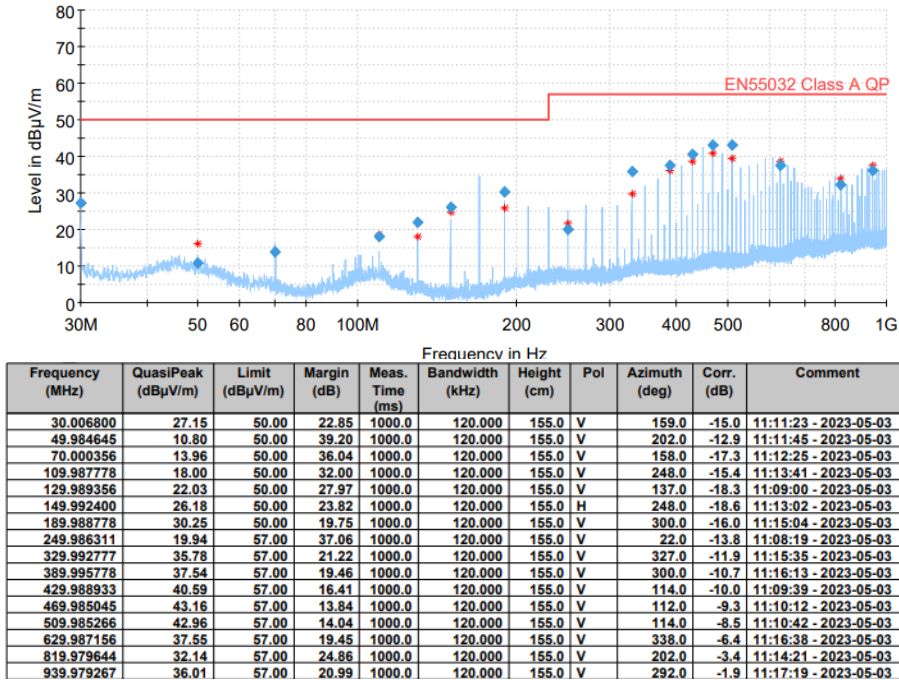


Figure A.3: Comb generator with ITO shielding from 30 MHz to 1 GHz. In the table, **Pol** means whether the antenna is angled vertically or horizontally.

A.3 With a Silver Film Shield

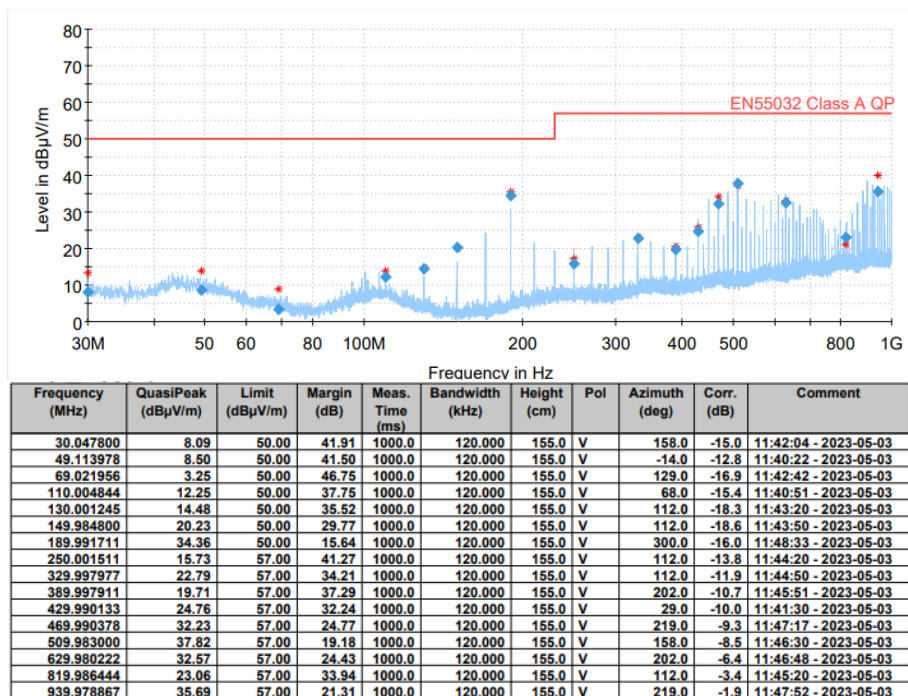


Figure A.4: Comb generator with silver film from 30 MHz to 1 GHz. In the table, *Pol* means whether the antenna is angled vertically or horizontally.

A.4 With a Galvanized Steel Mesh Shield

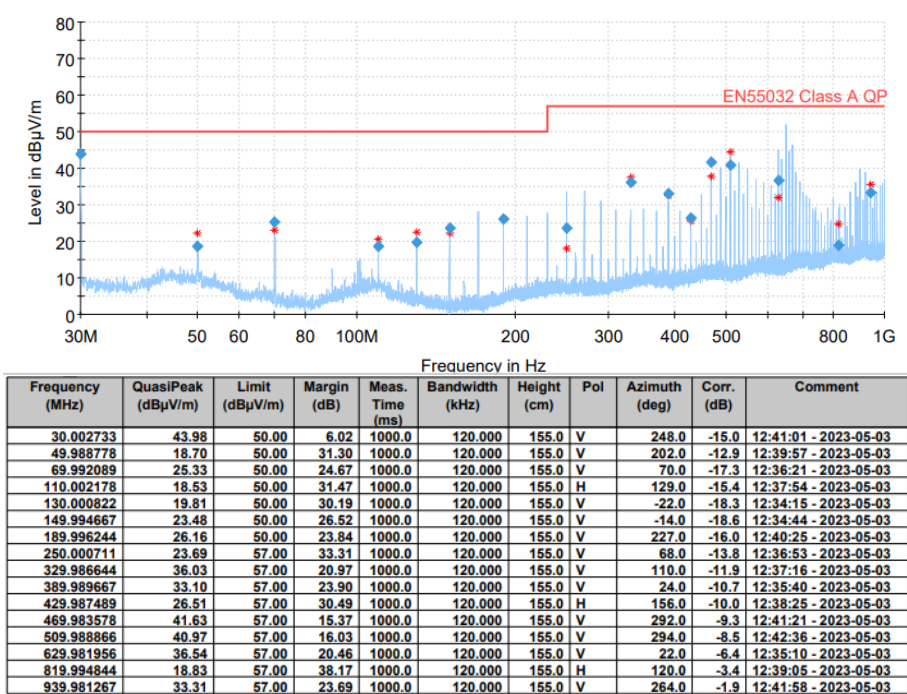


Figure A.5: Comb generator with galvanized mesh from 30 MHz to 1 GHz. In the table, **Pol** means whether the antenna is angled vertically or horizontally.

A.5 With an Aluminium Mesh Shield

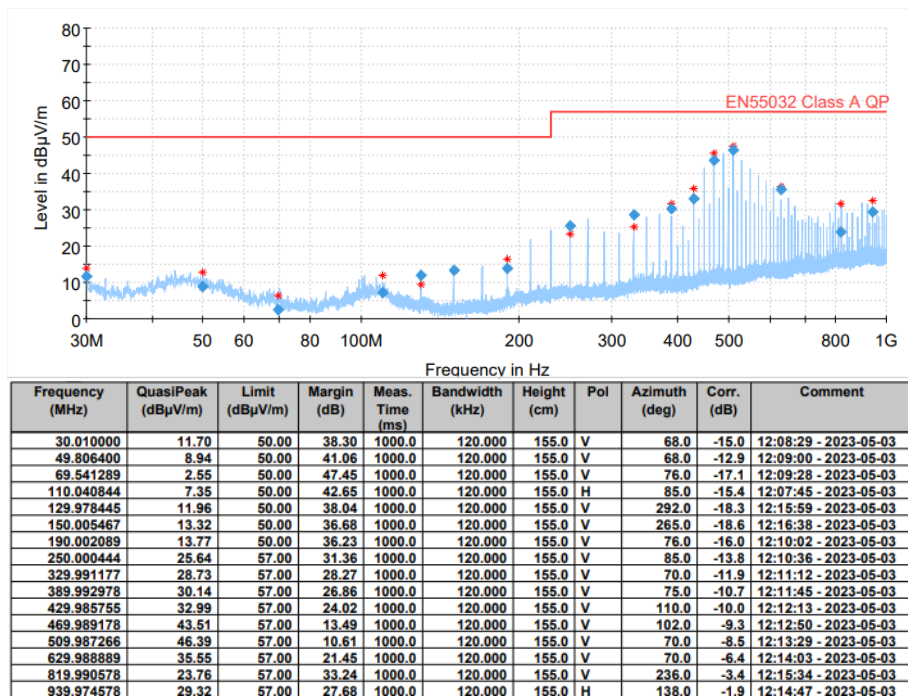


Figure A.6: Comb generator with aluminium mesh from 30 MHz to 1 GHz. In the table, **Pol** means whether the antenna is angled vertically or horizontally.

B Image Quality Photos

B.1 Visual Light Image With No Shield



Figure B.1: Visual light image with no shield attached.

B.2 Visual Light Image With ITO

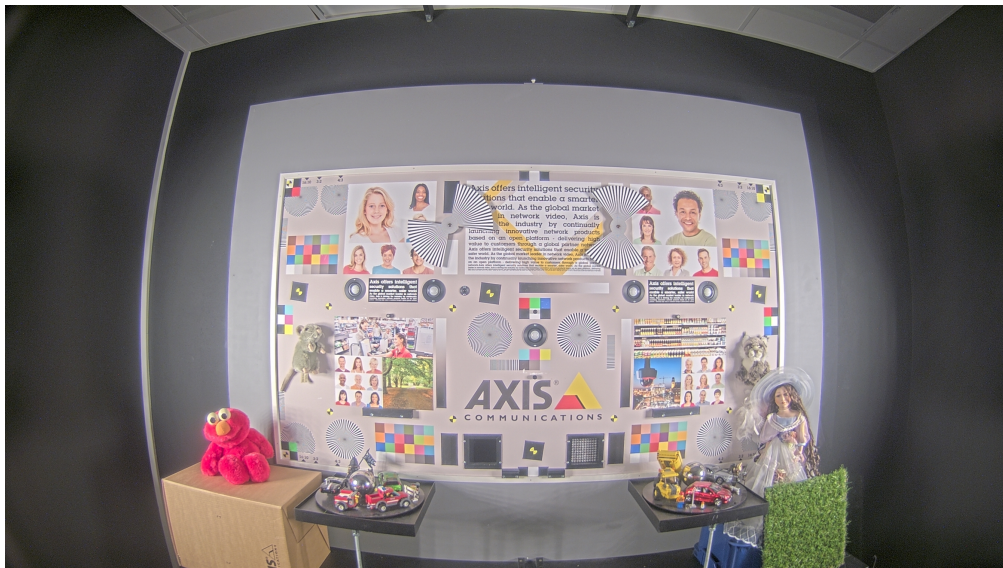


Figure B.2: Visual light image with ITO shield attached.

B.3 Visual Light Image With Silver Film



Figure B.3: Visual light image with silver shield attached.

B.4 Visual Light Image With Galvanized Steel Mesh



Figure B.4: Visual light image with galvanized mesh shield attached.

B.5 Visual Light Image With Aluminium Mesh



Figure B.5: Visual light image with aluminium mesh shield attached.

B.6 Infrared Light Image With No Shield



Figure B.6: Infrared light image with no shield attached.

B.7 Infrared Light Image With ITO

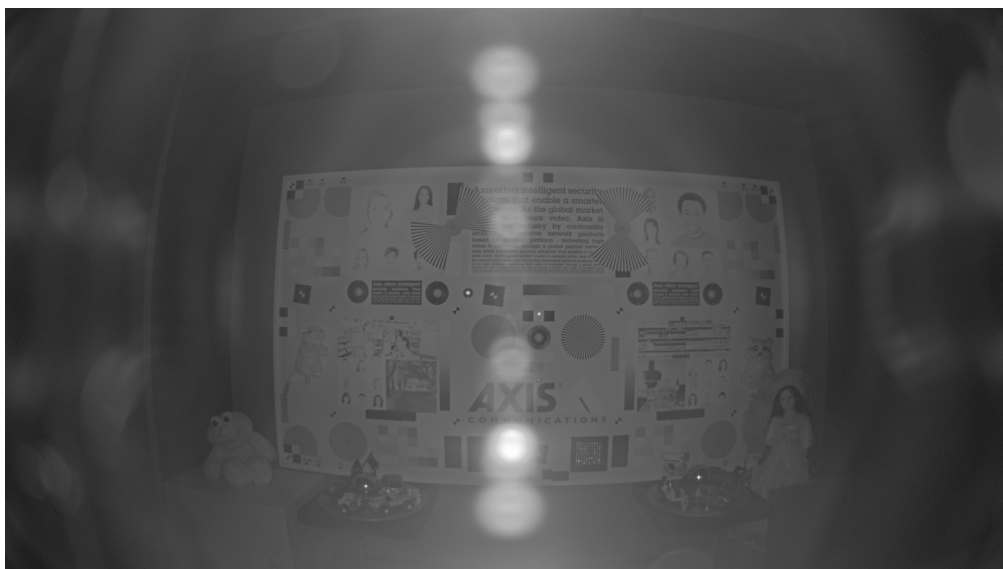


Figure B.7: Infrared light image with ITO shield attached.

B.8 Infrared Light Image With Silver Film

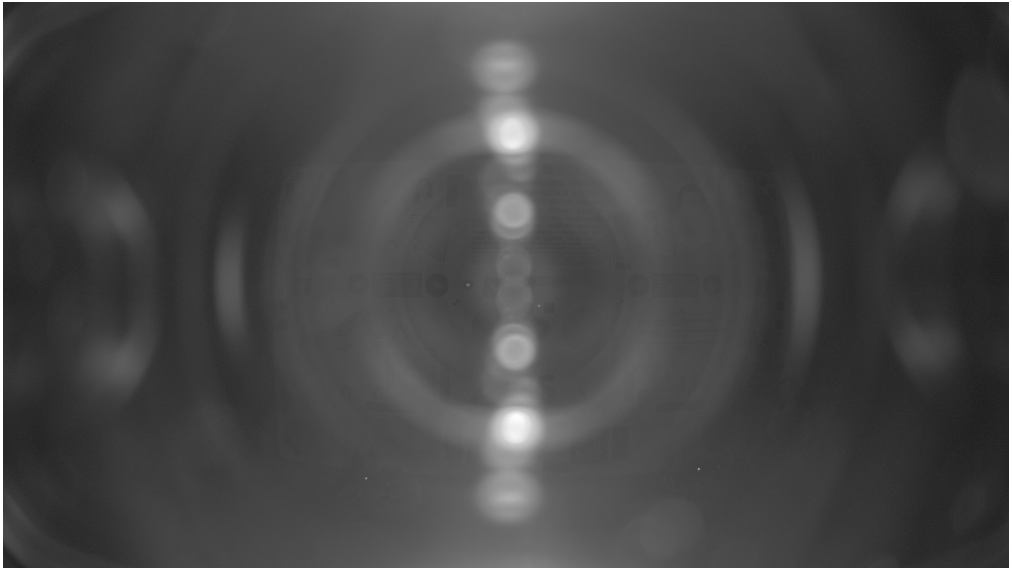


Figure B.8: Infrared light image with silver shield attached.

B.9 Infrared Light Image With Galvanized Steel Mesh



Figure B.9: Infrared light image with galvanized mesh shield attached.

B.10 Infrared Light Image With Aluminium Mesh

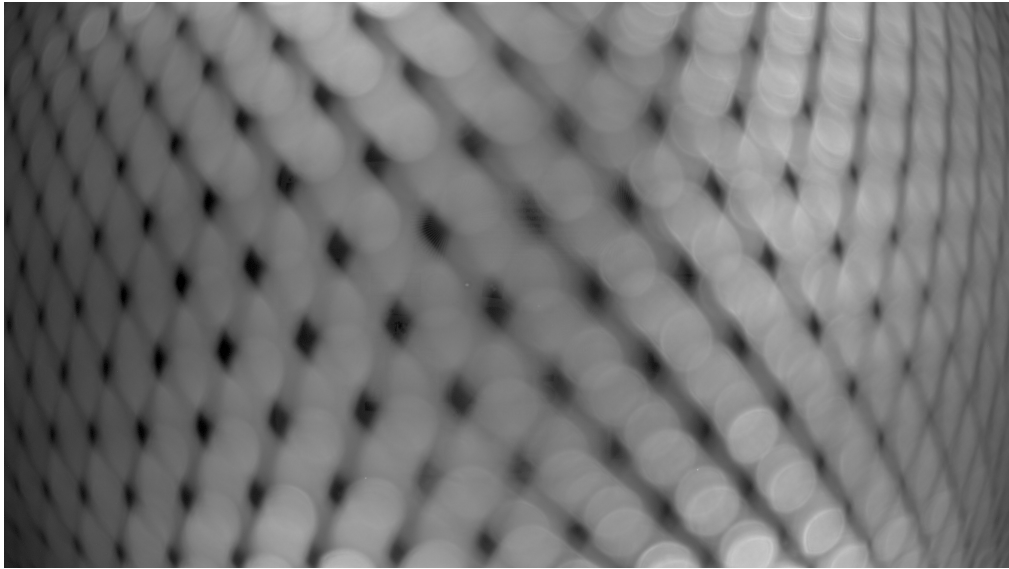


Figure B.10: Infrared light image with aluminium mesh shield attached.

C Camera Emission Graphs

C.1 Without a Shield

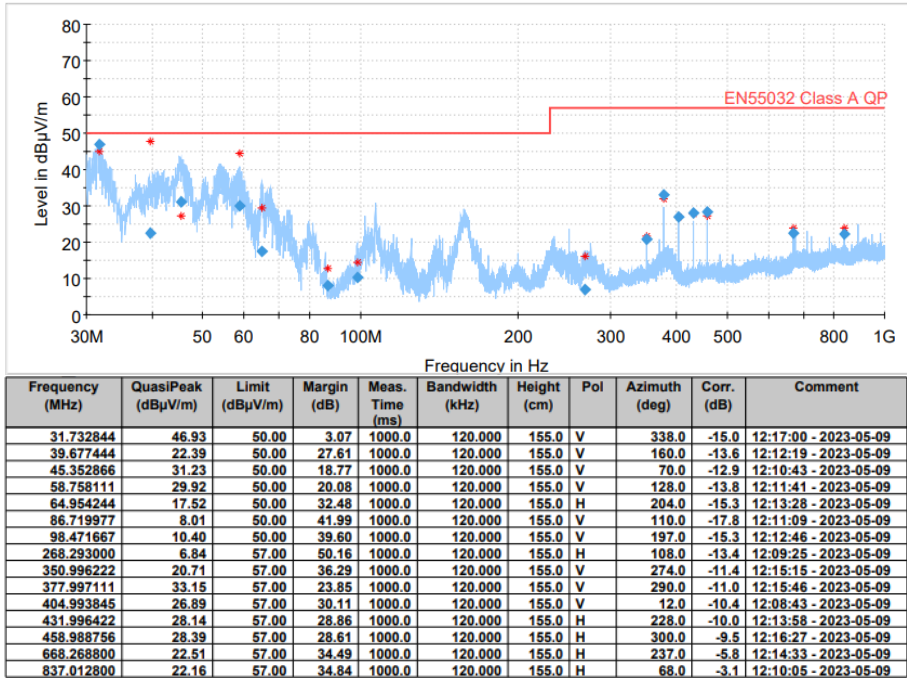


Figure C.1: Camera with no shielding from 30 MHz to 1 GHz. In the table, *Pol* means whether the antenna is angled vertically or horizontally.

C.2 With an ITO Film Shield

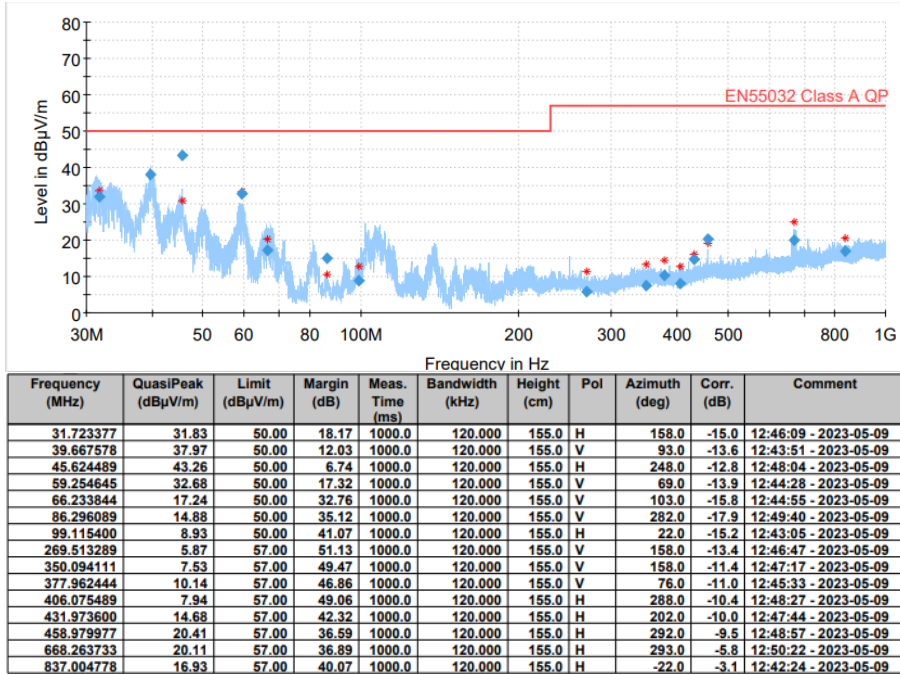


Figure C.2: Camera with ITO shielding from 30 MHz to 1 GHz. In the table, *Pol* means whether the antenna is angled vertically or horizontally.

C.3 With a Silver Film Shield

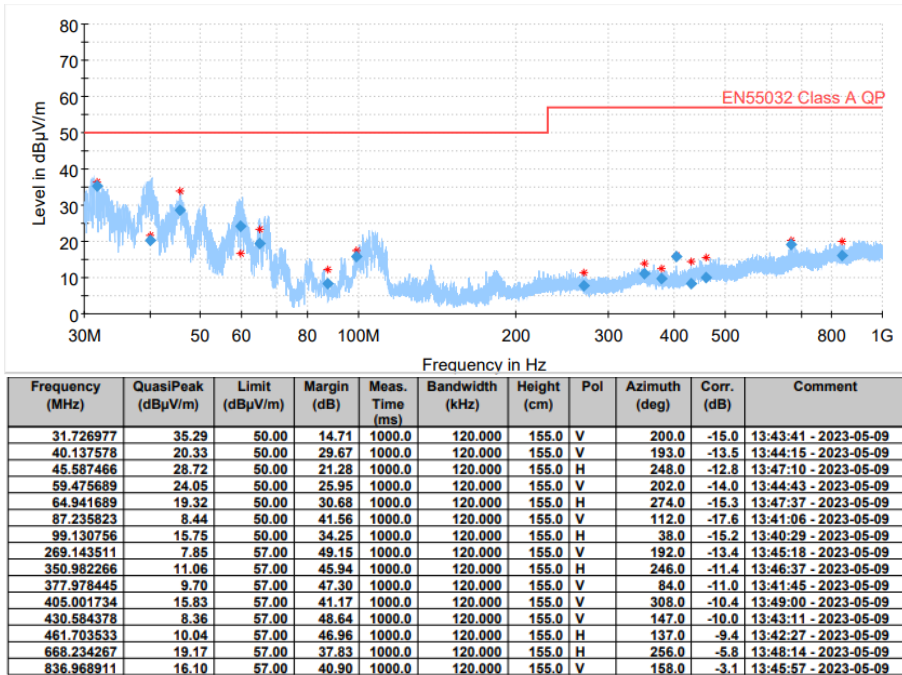


Figure C.3: Camera with silver film shielding from 30 MHz to 1 GHz. In the table, **Pol** means whether the antenna is angled vertically or horizontally.

C.4 With a Galvanized Steel Mesh Shield

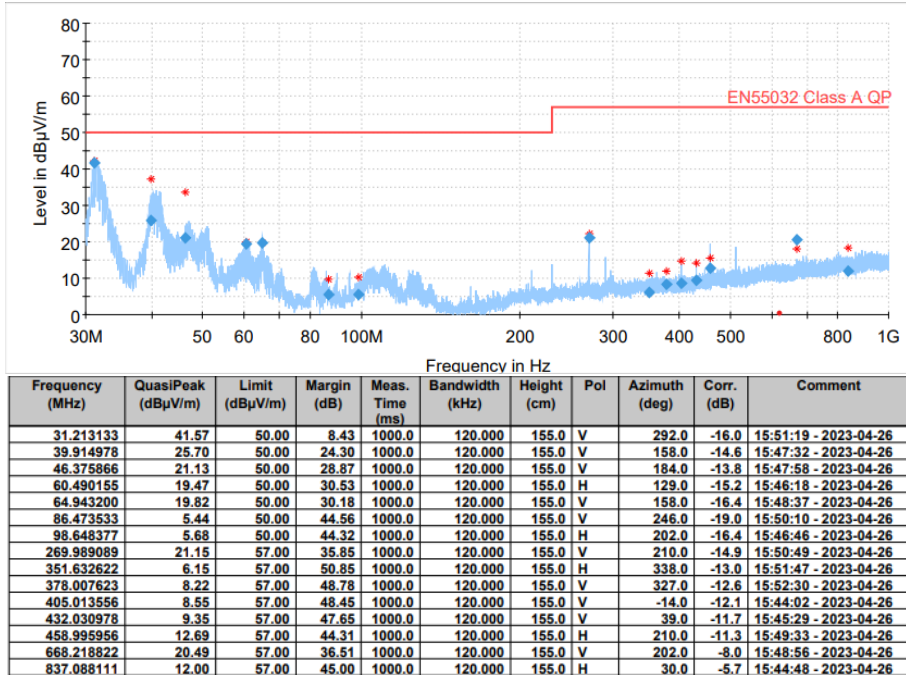


Figure C.4: Camera with galvanized steel mesh shielding from 30 MHz to 1 GHz. In the table, **Pol** means whether the antenna is angled vertically or horizontally.

C.5 With an Aluminium Mesh Shield

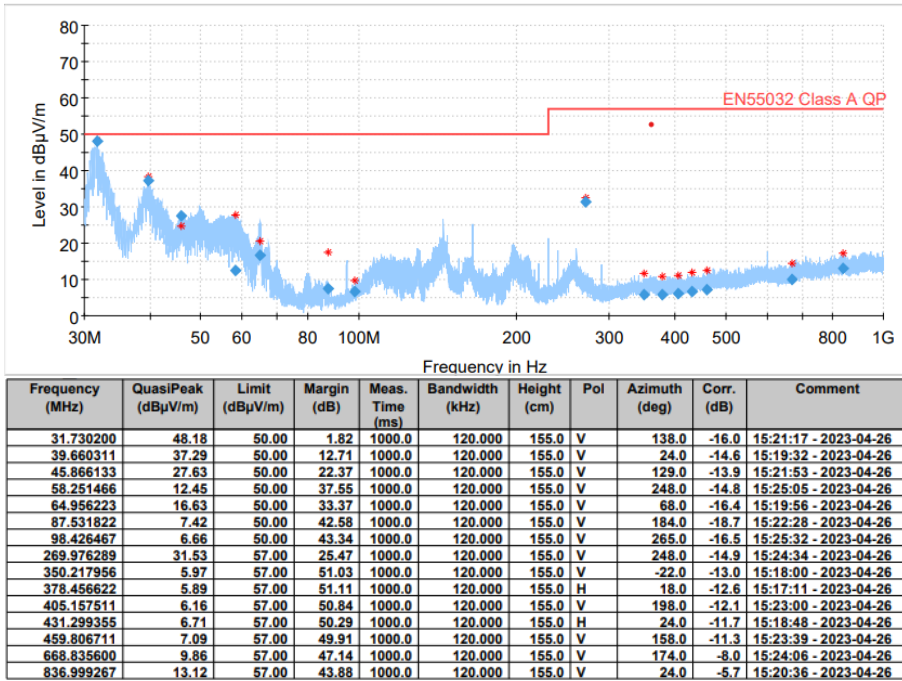


Figure C.5: Camera with aluminium mesh shielding from 30 MHz to 1 GHz. In the table, *Pol* means whether the antenna is angled vertically or horizontally.